

ANNUAL
REVIEWS **Further**

Click here to view this article's
online features:

- Download figures as PPT slides
- Navigate linked references
- Download citations
- Explore related articles
- Search keywords

Red Clump Stars

Léo Girardi^{1,2}

¹Osservatorio Astronomico di Padova – INAF, Padova 35136, Italy;
email: leo.girardi@oapd.inaf.it

²Laboratório Interinstitucional de e-Astronomia – LIneA, Rio de Janeiro, RJ-20921-400, Brazil

Annu. Rev. Astron. Astrophys. 2016. 54:95–133

First published online as a Review in Advance on
June 20, 2016

The *Annual Review of Astronomy and Astrophysics* is
online at astro.annualreviews.org

This article's doi:
[10.1146/annurev-astro-081915-023354](https://doi.org/10.1146/annurev-astro-081915-023354)

Copyright © 2016 by Annual Reviews.
All rights reserved

Keywords

stars: evolution, low mass, Hertzsprung-Russell and color-magnitude
diagrams, Galaxy: stellar content, surveys

Abstract

Low-mass stars in their core-helium-burning stage define the sharpest feature present in the color-magnitude diagrams of nearby galaxy systems: the red clump (RC). This feature has given rise to a series of methods aimed at measuring the distributions of stellar distances and extinctions, especially in the Magellanic Clouds and Milky Way Bulge. Because the RC is easily recognizable within the data of large spectroscopic and asteroseismic surveys, it is a useful probe of stellar densities, kinematics, and chemical abundances across the Milky Way disk; it can be applied up to larger distances than that allowed by dwarfs; and it has better accuracy than is possible with other kinds of giants. Here, we discuss the reasons for the RC narrowness in several sets of observational data, its fine structure, and the presence of systematic changes in the RC properties as regards age, metallicity, and the observed passband. These factors set the limits on the validity and accuracy of several RC methods defined in the literature.

Contents

1. INTRODUCTION	96
1.1. Overview and Brief History	96
1.2. Main Goals of This Review	97
2. BASIC THEORY	97
2.1. Basic Stellar Evolution: The RC in the Hertzsprung–Russell Diagram and Lifetimes	97
2.2. Basic Population Synthesis: Their Expected Mass and Age Distributions	103
2.3. Substructures: The Secondary RC, the Vertical Structure, and the Transition to the Horizontal Branch	105
3. THE RC OBSERVATIONS	106
3.1. The RC in Open and Metal-Rich Globular Clusters of the Milky Way	106
3.2. The Solar Vicinity RC from <i>Hipparcos</i>	107
3.3. The RC in Wide-Area Photometric Surveys of the Milky Way	109
3.4. The RC in Massive Spectroscopic Surveys	110
3.5. The RC in Massive Asteroseismic Surveys	110
3.6. The RC in Other Local Group Galaxies	114
3.7. The RC in Star Clusters of the Magellanic Clouds	116
4. REMARKS ABOUT POPULAR RC METHODS	118
4.1. RC Stars as Standard Candles	118
4.2. RC Stars as Extinction Probes	121
4.3. RC Stars as Density Probes	122
4.4. RC Stars as Kinematical and Chemical-Evolution Probes	124
4.5. RC Stars as Age Probes	124
5. OPEN ISSUES	125
5.1. How Good a Standard Candle Can the RC Ever Become?	125
5.2. Pending Stellar-Evolution Issues: Mixing in Late He-Burning Stages, Mass Loss, Rotation, and Binarity	126
6. CLOSING REMARKS	127

1. INTRODUCTION

1.1. Overview and Brief History

The clump of red giants (hereafter red clump, RC) is a striking feature in the color-magnitude diagrams (CMDs) of intermediate-age star clusters and nearby galaxies. It is made of low-mass stars in the stage of core He-burning (CHeB) that, owing to their sizable convective envelopes, appear red and close to the first-ascent red giant branch (RGB). Their sizable convective envelopes result from either a moderately high metallicity or, more generally, a significant buffer of mass (a few $0.1 M_{\odot}$) above the H-burning shell. Low-mass stars without such a buffer, or with extremely low metallicities, will burn He at higher effective temperatures, defining more extended features that we can refer to generically as the horizontal branch (HB). In the dichotomy between the RC and the HB, RC stars are obviously associated with younger and more metal-rich populations than those associated with the HB.

Although the RC is sometimes referred to as the “red extremity of the HB,” RC stars are far more abundant than HB stars. As we discuss later, in any star-forming galaxy observed to

RC: red clump

CHeB: core helium-burning

RGB: first-ascent red giant branch

HB: horizontal branch

sufficient depth RC stars are expected to make about 1/3 of all red giants. They likely make a similar fraction of the red point sources in wide-area IR surveys like Two Micron All-Sky Survey (2MASS), the UK Infrared Telescope's UK Infrared Deep Sky Survey (UKIDSS), Vista Variables in the Via Lactea (VVV), Galactic Legacy Infrared Mid-Plane Survey Extraordinaire (GLIMPSE), and Wide-Field Infrared Survey Explorer (WISE)—especially at the brighter magnitudes and close to the Galactic Plane, where the numbers of distant giants overcome those of intervening nearby dwarfs. RC stars also comprise a large fraction of the stars observed in present large spectroscopic surveys of the Milky Way (MW), such as Radial Velocity Experiment (RAVE), Apache Point Observatory Galactic Evolution Experiment (APOGEE), *Gaia*-ESO Survey (GES), GALactic Archaeology with HERMES (GALAH), and Large Sky Area Multi-Object Fiber Spectroscopic Telescope (LAMOST).

Despite their ubiquity, RC stars were virtually unknown until 45 years ago, contrary to their cousins, HB and RR Lyrae stars, which have been routinely studied in old globular clusters for more than a century (e.g., Bailey 1902). The first appearance of the term “clump of red giants” (later to become “red clump”) can be traced back to Cannon (1970), who compared the CMDs of a few intermediate-age clusters with the predictions from stellar-evolution models. In this seminal work, the RC was not only identified as a real CMD feature but also correctly interpreted as being the result of post-RGB evolution in low-mass stars. Cannon (1970) first suggested that the RC could provide crude distance and reddening estimates to their hosting clusters and that a large fraction of nearby field giants should actually be RC stars.

For many years the RC has been mentioned in studies of open clusters and Local Group galaxies and in theoretical work on stellar evolution, but rarely is it the main protagonist. Notable exceptions were a series of studies started by Gardiner & Hawkins (1991) in which the width of the RC was used to constrain the depth along different lines of sight to the Small Magellanic Cloud (SMC) galaxy, and the evidence for the Galactic Bar, which was derived from the RC luminosity variations across the Bulge by Stanek et al. (1994, 1997). The interest in the RC has sharply increased again after *Hipparcos* provided a large sample of such stars with very small parallax errors (about 600 with $\sigma_{\pi}/\pi < 0.1$), evincing how concentrated the RC is in the Hertzsprung-Russell diagram (HRD) and providing a reference point for the RC's use as a standard candle. Particularly important was the work by Paczyński & Stanek (1998), who demonstrated that the mean *I*-band intrinsic magnitude from *Hipparcos* was practically free from statistical uncertainties.

1.2. Main Goals of This Review

The ubiquity of RC stars and the near-constancy of their intrinsic properties are now widely recognized. This has given origin to a series of “red clump methods,” in which candidate RC stars are used as probes of stellar distances, extinctions, kinematics, and chemistry in many Local Group galaxies. As we discuss later, RC stars nowadays provide the primary methods to perform 3D mapping of stars and dust across the Magellanic Clouds and the MW Bulge. Thanks to all-sky photometric surveys, such as 2MASS (Skrutskie et al. 2006), and additional spectroscopy, candidate RC stars are being systematically used to probe kinematics and chemical abundance gradients across the MW disk.

Unfortunately, the recent burst in the use of RC stars does not appear to be followed by a widespread awareness about their nature and properties. Some very basic facts about RC stars are quite often ignored in the interpretation of observations, such as the unavoidable presence of population effects and their uneven age distribution in galaxies.

A primary goal of this review is to discuss these basic facts and the limitations of the several above-mentioned RC methods. Section 2 begins with a brief description of the basic

EAGB: early asymptotic giant branch

ZACHeB: zero-age CHeB

stellar-evolution and stellar populations theory necessary to interpret the RC observations. A more in-depth description of RC populations observed in the MW (disk and bulge) and in nearby galaxies follows in Section 3. This section also describes two recent advances in our knowledge of the RC, namely (*a*) the identification of the theoretically predicted fine structure of the RC, including the “secondary red clump,” in several data sets; and (*b*) the distinction between RC and RGB stars made possible by asteroseismology from the *Kepler* and the *Convection, Rotation & Planetary Transits* (CoRoT) satellites. Finally, keeping in mind the overall picture provided by present models and by a few key observations, RC methods for deriving distances, extinctions, and stellar densities are discussed in Section 4, as well as the use of RC stars as kinematical and chemical-evolution probes. We close with a brief discussion of the main theoretical uncertainties in the CHeB evolution associated with internal mixing, mass loss, rotation, and binarity (Section 5) and with perspectives on what may be found with the accurate observations of millions of RC stars by missions like *Gaia*, Large Synoptic Survey Telescope (LSST), *Wide Field Infrared Survey Telescope* (WFIRST), and new asteroseismic surveys (Section 6).

Most of these subjects are relatively new and not properly represented in previous Annual Reviews articles; they are mentioned briefly in the recent reviews by Gallart et al. (2005, about stellar evolution and CMDs) and Chaplin & Miglio (2013, about asteroseismology). RC stars are not discussed in the review of Galactic structure by Ivezić et al. (2012), which concentrates on results obtained from dwarfs using photometric parallaxes rather than from giants. However, RC stars are frequently mentioned by Bland-Hawthorn & Gerhard (2016, in this volume), as probes of the MW structure, chemical abundances, and kinematics.

2. BASIC THEORY

2.1. Basic Stellar Evolution: The RC in the Hertzsprung-Russell Diagram and Lifetimes

Most of the RC stars are low-mass stars in their stage of central He-burning. Their convective He-burning cores are surrounded by a radiative H-burning shell and by an H-rich convective envelope, as can be appreciated in the Kippenhahn diagram of **Figure 1**, which shows the evolution of a few quantities for a “typical RC star” of solar metallicity and an initial mass of $1.3 M_{\odot}$. The entire CHeB evolution consists in the gradual conversion of the He in the core into C and O, together with a modest outward migration of the H-burning shell. The same figure shows that during the CHeB evolution the bulk of luminosity is provided only by the H- and He-burning regions, with neutrino losses (not shown) being negligible and the gravitational luminosity (caused by contraction/expansion) being relevant only at the very end, as the He-burning region migrates from the He-exhausted core into a shell, and the star enters the phase of the early asymptotic giant branch (EAGB). The H-burning shell luminosity, L_H , initially dominates over the He-burning core luminosity, L_{He} , with the situation reversing at the second half of the CHeB phase; L_H and L_{He} conspire to produce a slowly increasing total luminosity, L , for most of the CHeB lifetime.

The basic theory of stellar structure and evolution is quite well developed for these low-mass CHeB configurations. The main theoretical uncertainties are linked to the following three aspects:

- The precise state—core and envelope mass, chemical profile, etc.—at which stars of different masses and metallicities enter into this evolutionary stage;
- The uncertain description of convective processes at the core border; and
- The uncertain rates of the key nuclear reaction $^{12}\text{C}(\alpha, \gamma)^{16}\text{O}$.

In this article, we refer to the initial stage of CHeB as the zero-age CHeB (ZACHeB), which is obviously an extension of the classical definition of the zero-age HB that applies to old

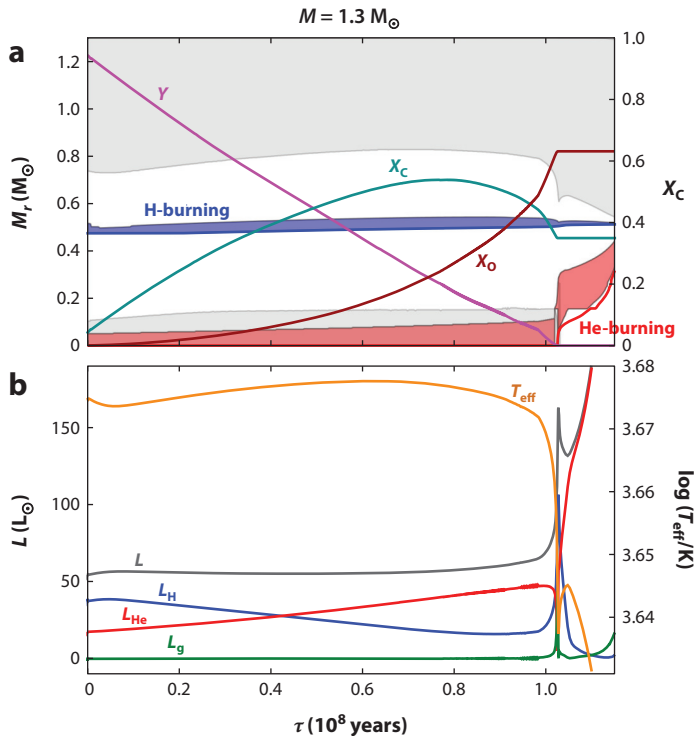


Figure 1

(a) Kippenhahn diagram showing the time evolution of a typical red clump star of mass $1.3 M_{\odot}$ and initial composition close to solar ($Z = 0.014$, $Y = 0.273$), taken from the PARSEC (Bressan et al. 2012) v1.2 suite of tracks. Regions of significant H- and He-burning luminosity are marked in blue and red, respectively, with the continuous lines indicating the limits of the H- and He-exhausted regions. Convective regions are marked in gray. The scale at the right axis indicates the evolution of the central mass fraction, X_c , of He, carbon, and oxygen. (b) The luminosity evolution for the same model distinguishing the total, H- and He-burning, and gravitational luminosity (L , L_H , L_{He} , L_g), plus the time evolution of $\log T_{\text{eff}}$.

low-mass stars. Whereas the stellar structure at the ZACHeB is a determinant for the entire CHeB evolution, the latter two processes—convection and nuclear reaction rates—affect mainly the very last fraction of this phase; they are discussed in Section 5.2.

The main parameters determining the luminosity of CHeB stars are the core and the envelope masses, which are set by the evolution previous to the ZACHeB. The core mass at He ignition, M_{core}^0 (see the sidebar The Core Mass at Helium Ignition), presents a plateau for all low-mass stars, which develop electron-degenerate cores after the main sequence (MS; **Figure 2**). These stars have greater pressure support, and their centers are cooled by high electron conductivity and (to a lesser extent) by plasma neutrinos; hence, their He ignition is delayed, and they follow the evolution along the RGB. Their cores accrete ashes from the H-burning shell until a mass of about $0.47 M_{\odot}$ is reached; at this point, He ignites off-center in a flash, leading to the progressive lifting of core degeneracy in a few subflashes that last for less than 2 Myr (Thomas 1967, Bildsten et al. 2012). 2D and 3D hydrodynamic models confirm that the He-flash phase does not significantly alter the stellar structures (Mocák et al. 2009), validating the approximations generally used to build ZACHeB models of low-mass stars in stellar-evolution codes.

Instead, in the contracting core left after the MS of slightly more massive stars, electron degeneracy is prevented by the central He ignition and its consequent core expansion. The star

MS: main sequence

THE CORE MASS AT HELIUM IGNITION

Although the general appearance of the $M_{\text{core}}^0(M_i)$ curve in **Figure 2** has been confirmed by dozens of independent calculations over the past few decades (see Sweigart et al. 1990, Castellani et al. 2000, Girardi et al. 2013), two aspects are as yet not completely settled:

1. What is the maximum initial mass for a star to avoid He degeneracy, hence leading to the minimum value of M_{core}^0 of $0.33 M_\odot$? This initial mass defines the separation between low- and intermediate-mass stars and depends on the amount of convective mixing occurring during the MS (Bressan et al. 2015). We refer to this limiting mass as the He-flash limit, or M_{HeF} , although the precise definition of this quantity varies somewhat in the literature. For classical models of near-solar metallicity, M_{HeF} is close to $2.5 M_\odot$, whereas the models with a moderate efficiency of convective overshooting favored nowadays present M_{HeF} values generally between 1.7 and $2.0 M_\odot$ (e.g., Castellani et al. 2000). M_{HeF} also depends mildly on the initial chemical composition (e.g., Sweigart et al. 1990, Bressan et al. 2012; and **Figure 2**).

2. How sharp is the transition in M_{core}^0 occurring in the vicinity of M_{HeF} ? Many grids of stellar tracks in the past indicated a transition occurring over a range of initial masses smaller than $\sim 0.1 M_\odot$ —corresponding to a relatively small range of stellar population ages (Sweigart et al. 1990). However, the latest models computed with very high resolution in mass (Girardi et al. 2013) indicate a sharp discontinuity in M_{core}^0 , which drops quickly from $M_{\text{core}}^0 > 0.40 M_\odot$ down to $\sim 0.35 M_\odot$ in less than $0.01 M_\odot$. This drop is caused by the H-exhausted core having to choose between two distinct evolutionary paths: Either the core is quickly cooled by electron degeneracy or quickly heated by triple-alpha reactions. If confirmed by independent models, this sharp feature would provide an unambiguous definition of M_{HeF} .

settles on the quiescent He-burning stage with a core mass that, at least for models with moderate core overshooting, is determined by the previous convective core during the MS. Thus, M_{core}^0 turns out to be nearly proportional to the stellar mass, as illustrated in **Figure 2**.

The presence of a plateau in M_{core}^0 for all $M_i < M_{\text{HeF}}$ —covering a wide range of turnoff ages—is the reason why low-mass CHeB stars appear as a clump in the CMD of galaxies, and it is also the reason for its near constancy among intermediate-age star clusters: Because their core masses are very similar, differences in L and T_{eff} are limited to those allowed/caused by their different envelope masses and compositions. **Figure 3a** shows the HRD of CHeB tracks over a wide range of masses and metallicities. As can be seen in the top panels, model ZACHeB stars with $M_i < M_{\text{HeF}}$ of a given metallicity have their $\log L$ confined within a range of $\lesssim 0.2$ dex. Even so, much of this variation is caused by the lowest-mass stars, with $M_i \lesssim 0.7 M_\odot$, which, due to their small envelope masses, places them at the transition between the RC and the HB. For a given metallicity and excluding the HB section of the HRD, ZACHeB effective temperatures are confined to within ~ 450 K or 0.04 dex in $\log T_{\text{eff}}$.

For stars with $M_i > M_{\text{HeF}}$, the ZACHeB luminosity monotonically increases with the stellar mass, as expected from the behavior of the core mass (**Figure 2**). However, the minimum value of $M_{\text{core}}^0 = 0.33 M_\odot$ at $M_i = M_{\text{HeF}}$ causes these stars—at least those between M_{HeF} and $M_{\text{HeF}} + 0.3 M_\odot$ —to be fainter than the RC stars of smaller masses. Whenever such stars are present in a stellar population, they cause the appearance of the secondary red clump (SRC) in the HRD, that is, an appendix of CHeB stars extending down to 0.15 dex in luminosity (0.4 mag) from the main (or “classical”) RC of low-mass stars (Girardi 1999). Stars more massive than $M_{\text{HeF}} + 0.3 M_\odot$ are slightly brighter than the RC and, hence, define another feature, the vertical structure (VS), which is a tail of brighter and more massive CHeB stars departing directly from the SRC. Although caused by stars with a distinct evolutionary history, the SRC feature and a fraction of

SRC: secondary red clump

VS: vertical structure

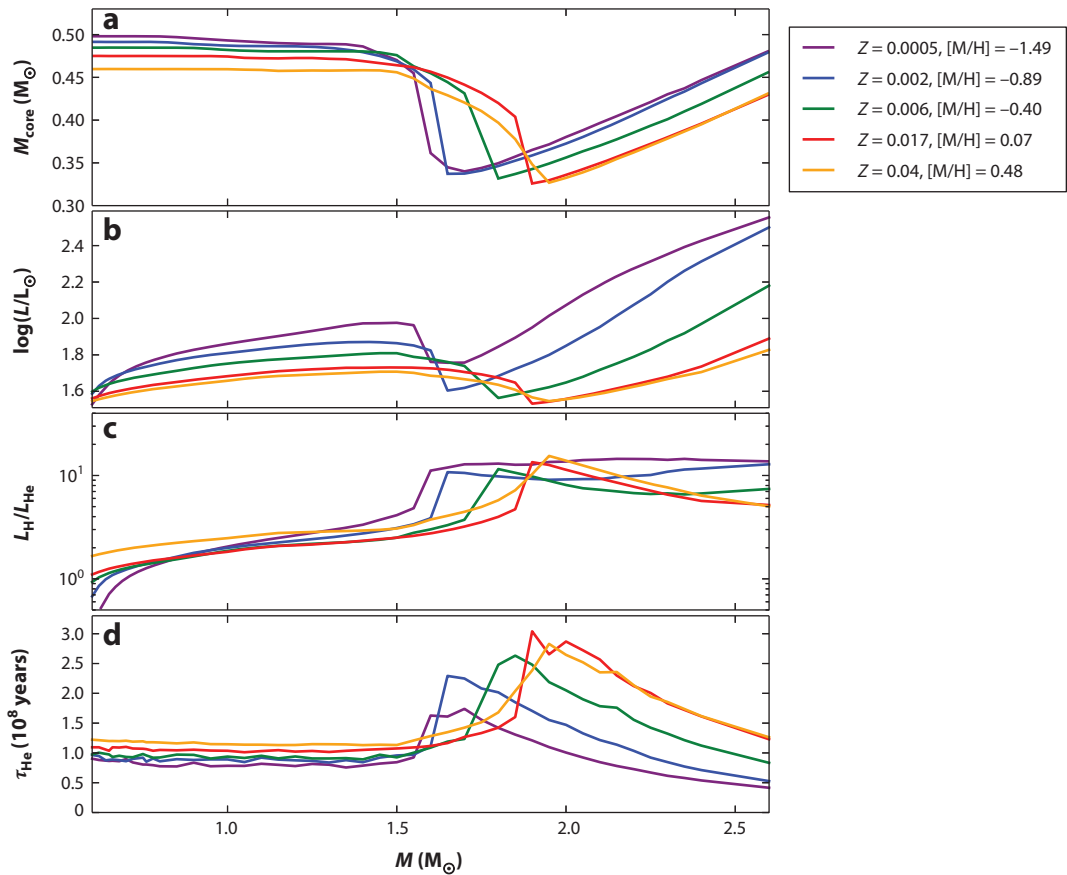
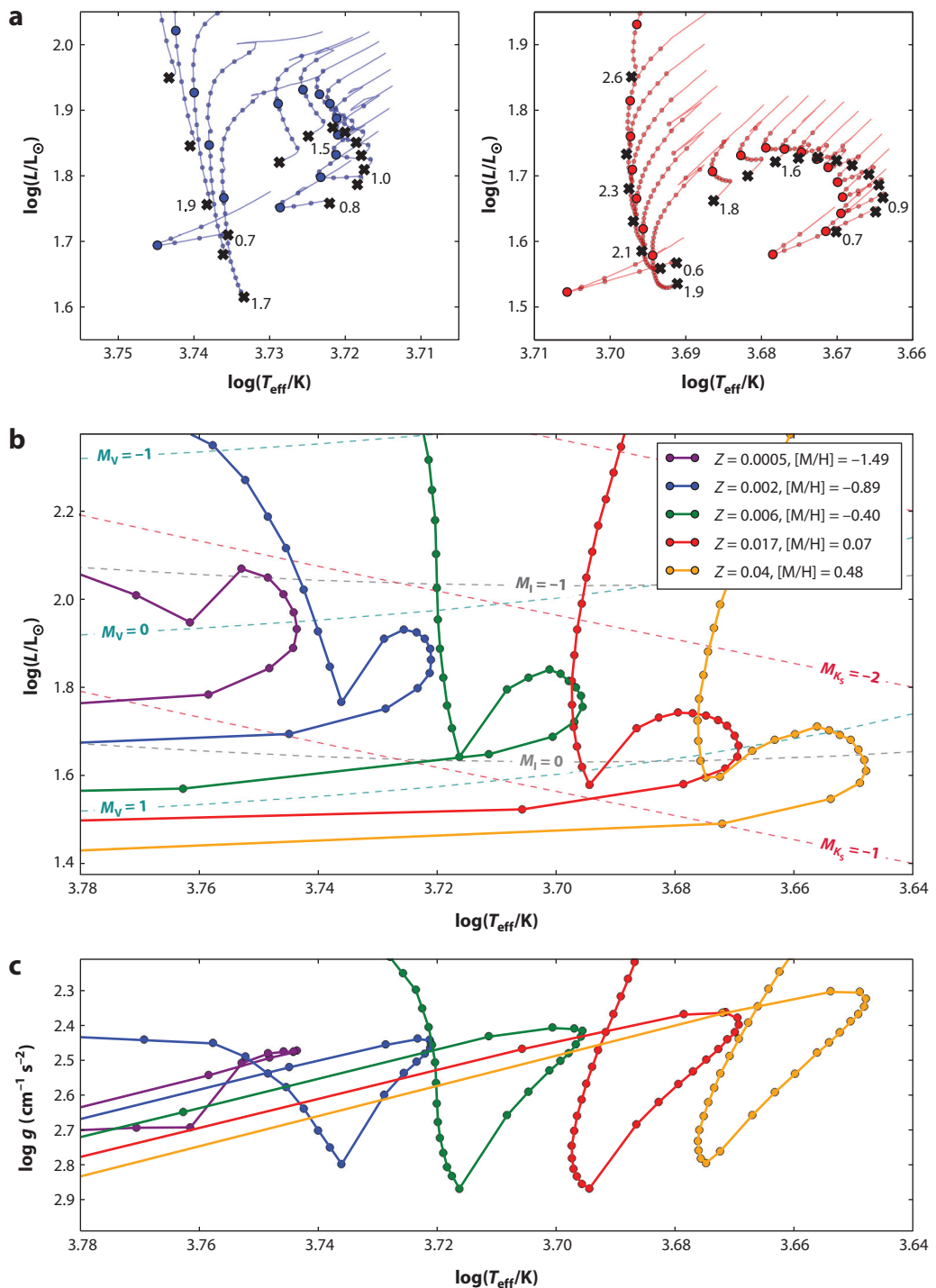


Figure 2

Some crucial parameters at the beginning of the core helium-burning (CHeB) lifetime as a function of mass and metallicity and for the entire mass interval relevant for the definition of the red clump. This stage is defined as the point where just 5% of the available central He is already burnt by triple-alpha reactions; this criterion ensures uniformity in the plot by avoiding the initial phase of stellar contraction that follows He ignition. Panels show (a) the H-exhausted core mass M_{core} , (b) the total stellar luminosity L , and (c) the ratio between the luminosities provided by the H-burning shell and the He-burning core $L_{\text{H}}/L_{\text{He}}$. Panel *d* shows the total CHeB lifetimes, τ_{He} . Irregularities in the plot appear for all quantities in the vicinity of M_{HeB} as a result of the finite mass resolution of the grid and in the τ_{He} as a result of minor episodes of core expansion occurring at the end of the CHeB lifetime.

the VS are located close enough to the main RC to be inextricably associated with it and, in many cases, observationally indistinguishable from it (see Section 3). Note that the internal structure and evolution of these CHeB stars are not dissimilar to those of typical RC stars of smaller mass, their main distinguishing feature being the dominance of H-burning over He-burning luminosity, which lasts for most of their evolution.

The above description refers to how stars of different masses position themselves in the HRD when at their ZACHeB stage. What follows next for each star is, generally, a modest evolution upward in luminosity as He is converted into C and O (**Figure 1**). At the same time, the T_{eff} initially increases, then later decreases toward the end of central He-burning. The total extent of this evolution depends on the description adopted for convective processes and on the $^{12}\text{C}(\alpha, \gamma)^{12}\text{O}$ reaction rate (see Section 5.2); for models with moderate convective core overshooting and rates



presently favored by most authors, this excursion is generally limited to within ~ 0.1 dex in luminosity and ~ 0.01 dex in T_{eff} (**Figure 3a**) during the $\sim 10^8$ years of the CHeB lifetimes of low-mass stars (**Figure 2d**). However, stars slightly more massive than M_{HeF} , having started their He-burning life at lower luminosities with smaller core masses, develop a much longer excursion in L , resulting in a CHeB lifetime that is between 2.5 and 3 times longer than that in low-mass stars (**Figure 2**). As illustrated by Girardi et al. (2013), this latter trend is shared by most grids of stellar models published in the past 30 years, although they strongly differ in terms of input physics and mass resolution.

Figure 3b shows the median-age location of every CHeB track in the HRD for stars in a much wider range of metallicities than those in the top panels. Assuming a typical $\log g = 2.5$ for RC stars and bolometric corrections derived from the Castelli & Kurucz (2003) library of synthetic spectra for $[\text{Fe}/\text{H}] = -0.5$, we can derive the lines of constant magnitudes in several passbands, shown in the plot, which are discussed later in Section 4.1. The slope of these lines changes systematically with the mean wavelength being sampled; however, we note that it changes little for passbands redward of K_s .

Figure 3c shows the same sequences of median-age CHeB models in the $\log g \times \log T_{\text{eff}}$ plane, which is more suitable for comparisons with spectroscopic data. Considering the stellar evolution and the total range of metallicities plotted in the figure, the total range of $\log g$ covered by the main RC is of the order of just 0.5 dex. At low metallicities, this $\log g$ range is further narrowed down to 0.2 dex or 0.3 dex. Interestingly, for high metallicities a larger range of intermediate masses appears close enough to the RC to be considered as genuine RC members in this diagram. Indeed, whereas in the HRD the SRC was defined by stars having masses between M_{HeF} and $M_{\text{HeF}} + 0.3 M_{\odot}$, in the $\log g \times \log T_{\text{eff}}$ plane CHeB stars as massive as $M_{\text{HeF}} + 1.3 M_{\odot}$ appear in the same $\log g$ range as the low-mass RC. Therefore, we might expect the SRC feature to be more prominent in such diagrams than in the HRD and in CMDs.

2.2. Basic Population Synthesis: Their Expected Mass and Age Distributions

The discussion above suffices to describe the RC expected mean position and morphology in the HRD in the case of star clusters (but see Section 3.7), where all RC stars can be assumed to have the same initial mass and, hence, closely follow the small evolutionary paths drawn in **Figure 3a**. To describe the RC in resolved galaxies, we have to consider in addition the expected mass (hence age) distribution of RC stars and their metallicity distribution. For this, we can follow the steps illustrated by Girardi et al. (1998) and Girardi (1999) using the basic theory of stellar

Figure 3

(a) Sets of core helium-burning (CHeB) evolutionary tracks extracted from the PARSEC database (Bressan et al. 2012), in the Hertzsprung-Russell diagram (HRD), for initial metallicities corresponding roughly to those of intermediate-age populations in the Small Magellanic Cloud and Solar Neighborhood ($Z = 0.002$ and $Z = 0.017$, respectively). The tracks cover the mass range between ~ 0.6 and $\sim 2.6 M_{\odot}$ (depending on metallicity) and are regularly spaced by $0.1 M_{\odot}$ for all $M < 2.5 M_{\odot}$. A few mass values are indicated for reference; we note that M_{HeF} is located close to $1.7 M_{\odot}$ for $Z = 0.002$ and to $1.9 M_{\odot}$ for $Z = 0.017$. Each track covers the total quiescent CHeB lifetime (in which $L_{\text{He}} > 0$ and $|L_g|/L < 0.005$), starting at the black cross—which we refer to as being the zero-age CHeB. Small dots are positioned at equally spaced age intervals of 10^7 years along the tracks, giving an idea of the total CHeB lifetimes and of the regions in the HRD expected to be more densely populated with stars. For each track, the bigger colored dot marks the median age, located at halfway in the CHeB lifetime. (b) The same as above but now showing only the median-age position of CHeB tracks (i.e., the big colored dots in panel a), so as to draw their overall distribution in the HRD as a function of stellar mass, and for a wide range of metallicities. The additional dashed lines mark the approximate loci of constant absolute magnitudes in the passbands V , I , and K_s . (c) The same median-age CHeB sequences in the $\log g \times \log T_{\text{eff}}$ plane.

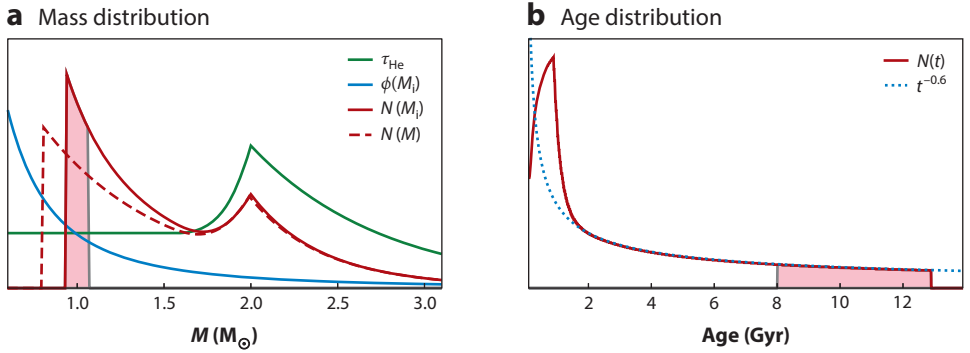


Figure 4

(a) The mass distribution of core helium-burning stars, $N(M_i)$, for a galaxy with a constant star-formation rate between now and 12.5 Gyr ago (red thick line) and the functions that determine it, $\tau_{\text{He}}(M_i)$ and $\phi(M_i)$. The red dashed line illustrates the effect of first-ascent red giant branch mass loss; i.e., it shows the distribution of actual masses, $N(M)$. The shaded pink area shows $N(M_i)$ for a galaxy that suddenly stopped forming stars 8 Gyr ago. (b) The implied age distributions, compared with the $t^{-0.6}$ function.

populations for post-MS stars (see, e.g., Tinsley 1980, Renzini & Buzzoni 1986) and approximate the distributions of masses and ages of CHeB stars by

$$N(M) \propto \phi(M_i) \times \psi[t - \tau_H(M_i)] \times \tau_{\text{He}}(M), \quad (1)$$

$$N(t) \propto \phi(M_i) \times \left| \frac{d\tau_H(M_i)}{dM_i} \right|^{-1} \times \psi[t - \tau_H(M_i)] \times \tau_{\text{He}}, \quad (2)$$

where $\phi(M_i) = dN/dM_i$ is the initial mass function (IMF) by number; $\psi[t - \tau_H(M_i)]$ is the star-formation rate (SFR) at the age at which the stars were formed; $\tau_H(M_i)$ is the MS lifetime; and τ_{He} is the CHeB lifetime. $\phi(M_i) \times |d\tau_H(M_i)/dM_i|^{-1} \times \psi[t - \tau_H(M_i)]$ is the rate at which stars leave the MS. These distributions are schematically drawn in **Figure 4** for the case of a constant SFR, taking place between now ($t = 0$) and the largest possible lookback times ($t = 12.5$ Gyr), and a Salpeter (1955) IMF ($\phi(M_i) \propto M_i^{-2.35}$). Alternatively, we limit the same curves for a purely old population of ages between 8 and 12.5 Gyr and illustrate the effect of a modest integrated loss of mass on the RGB, $\Delta M(M_i)$. This mass loss changes the mapping between the actual and initial masses of the observed RC stars, but it has essentially no consequence for their evolution and does not affect their age distribution.

Galaxies with SFRs different from constant can have their RC age distribution derived by multiplying the SFR by the function depicted in **Figure 4b**. A particular case is that of quiescent galaxies, i.e., those which stopped their star formation a few gigayears ago. For them, the function is well described by a simple $t^{-0.6}$ law, and the age distribution of RC stars is given by $N(t) \propto \psi(t - \tau_H) \times t^{-0.6}$. For ages between 8 and 12.5 Gyr, $t^{-0.6}$ varies by less than 30%; this is essentially the only case for which the numbers of observed RC stars could provide a direct indication about the total SFR of a galaxy, within this level of uncertainty.

In the more general case of galaxies that have continuously formed stars over their entire history, the mass distribution presents two peaks caused by (a) the stars with the lowest mass having evolved away from the MS, and (b) the stars at $M_i \simeq M_{\text{HeF}}$ that present a marked peak in their CHeB

IMF: initial mass function

SFR: star-formation rate

lifetimes. However, the age distribution of RC stars is single-peaked with a pronounced maximum at the ages that correspond to $M_i \simeq M_{\text{HeF}}$. Importantly, this ensures that, in any galaxy with a relatively constant SFR over gigayear scales, the mean age of the RC will be relatively young and located, indicatively, somewhere between 1 and ~ 4 Gyr.

Notice also that Equations 1 and 2 derive from approximations that break down if τ_{He} becomes comparable with τ_H . Indeed, RC stars of $M_i \simeq M_{\text{HeF}}$ have $\tau_{\text{He}}/\tau_H \simeq 0.3$, which is the largest such ratio reached by red giants of any kind. For this reason, use of these equations should be limited to drawing general trends, as we do in this article. For the detailed work of population synthesis of galaxies, the preferred method is based on the construction of detailed isochrones and the identification of RC stars along them. Girardi & Salaris (2001) published tables with the photometric properties of the RC as a function of both age and metallicity (t, Z),

$$\langle M_\lambda(t, Z) \rangle = -2.5 \log \left[\frac{1}{N_{\text{RC}}(t, Z)} \int^{\text{CHeB}} \phi(M_i) 10^{-0.4M_\lambda} dM_i \right], \quad (3)$$

where $N_{\text{RC}}(t, Z)$ is the expected number of RC stars for each unit mass of stars formed in a single-burst stellar population:

$$N_{\text{RC}}(t, Z) = \int^{\text{CHeB}} \phi(M_i) dM_i. \quad (4)$$

The IMF, $\phi(M_i)$, is normalized to a total single-burst stellar population mass of $1 M_\odot$, and the integral is performed over the isochrone section corresponding to the CHeB phase. From the grid of $N_{\text{RC}}(t, Z)$ values, it is very easy to rederive the expected mean properties of RC stars in model galaxies—like the mean absolute magnitudes, $\langle M_\lambda \rangle$ —by simply averaging these properties with weighting factors given by N_{RC} times the adopted SFR and considering metallicities drawn from the age-metallicity relation (AMR) (Girardi & Salaris 2001). Alternatively, the same properties can be derived after producing synthetic samples of giants with codes such as TRILEGAL (Girardi et al. 2005) and IAC-star (Aparicio & Gallart 2004).

The first panel in **Figure 5** shows the result of the integral in Equation 4 as a function of age and metallicity, for a particular grid of isochrones characterized by its fine resolution in both initial mass and metallicity. It can be noticed that indeed N_{RC} varies by a factor of 10 between its maximum at 1.5 Gyr (and slightly below-solar metallicities) and its minimum at the oldest possible ages.

2.3. Substructures: The Secondary RC, the Vertical Structure, and the Transition to the Horizontal Branch

Joining the HRDs of single-mass RC stars with their mass/age distributions, as discussed in the previous two subsections, one can easily reach the following conclusions:

In galaxies with continuing star formation that follow a normal AMR (in which only stars older than a few gigayears have a metallicity significantly smaller than the presently forming ones), the RC contains significant structure, with the presence of a main “classical” RC, a marked SRC, a feeble VS, and—if the oldest stars are also metal poor—an extension toward the HB. Among these features, the VS and HB naturally define the boundaries of what can be considered as belonging to the RC: They are little populated because of the reduction of both τ_{He} and the IMF, and the wider range of magnitudes for more massive stars, and because of the small interval of initial masses corresponding to the HB. The SRC instead is a more marked feature, present whenever ~ 1 -Gyr-old stellar populations are present—except at very low metallicities (Girardi 1999). To show such fine RC features, synthetic HRDs should be based on evolutionary tracks covering

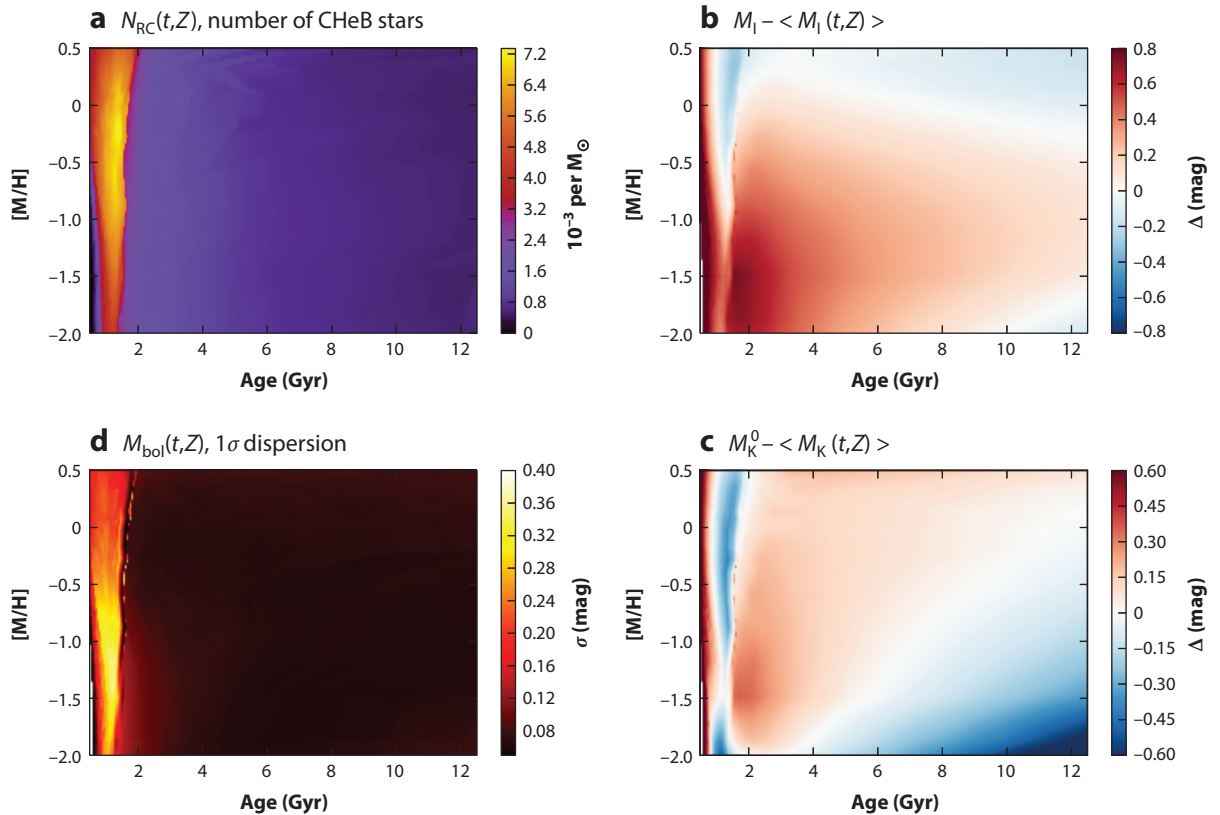


Figure 5

Some theoretical predictions for the behavior of core helium-burning (CHeB) stars as a function of age and metallicity, as derived from the PARSEC v1.2S suite of isochrones (Bressan et al. 2012), and adopting the Kroupa (2002) initial mass function, and no mass loss on the first-ascent red giant branch. (a) N_{RC} ; (b) the mean I -band magnitude as compared with a reference value from *Hipparcos* (namely the one by Francis & Anderson 2014, see Table 1 below), with model values being brighter/fainter in red/blue areas; (c) the same for the K -band; (d) the 1σ spread in the bolometric luminosity. Given the small T_{eff} range covered by the red clump (RC) stars in every isochrone, the 1σ spread will be similar in passbands such as V and I .

sufficiently wide intervals of mass and metallicity. Moreover, because the SRC corresponds to a limited range of stellar masses, its appearance in the HRD also depends on the mass resolution of the tracks computed in the vicinity of M_{HeF} (Girardi 1999).

However, in quiescent galaxies the RC is expected to be featureless except for the RC–HB transition, whose details depend on the adopted SFR and AMR at old ages and on the efficiency of RGB mass loss. But, in principle, there is no reason for the RC to be a sharp CMD feature even for quiescent galaxies and old bulges, unless the age-metallicity intervals being covered are really small.

How these features appear in CMDs depends on the passbands involved. A few lines of constant absolute magnitude in the V , I , and K passbands are drawn in Figure 3a. They translate in the maps of varying $\langle I \rangle$ and $\langle K \rangle$ that are shown in Figure 5b,c, which are used in the discussion of Section 4.1.

3. THE RC OBSERVATIONS

The theoretical considerations of Section 2 are quite general and should form the basis for the interpretation of RC data, much as similar relations (e.g., the mass-luminosity-age relation for the MS stars, the mass–radius and initial–final mass relations for white dwarfs, etc.) are the key to interpret the distributions of other kinds of stars. In practice, however, rarely has this theory been used, and rarely have their basic predictions been directly verified. This happens because of the compact nature of the RC, which is often completely blurred in CMDs by effects such as photometric errors, differential reddening, metallicity dispersion, and depths along the observed lines of sight. In this section, we review the many high-quality data (of various kinds) for RC stars in the Local Group and how they relate to this theory.

3.1. The RC in Open and Metal-Rich Globular Clusters of the Milky Way

Due to their modest present masses, open clusters in the MW typically present just a handful of RC stars, like the 7 RC members in M67 (with 3.5 Gyr; Sandquist 2004), the 4 in Berkeley 32 (~ 6 Gyr; D’Orazi et al. 2006), and the 3 stars “likely forming a RC” in NGC 188 (~ 7 Gyr; Sarajedini et al. 1999). A few other examples are presented by Mermilliod et al. (2008) and Mermilliod & Mayor (1990). These small numbers are perfectly in line with those expected from the theoretical isochrones for $\sim 10^4 M_{\odot}$ clusters following a Kroupa (2002) IMF (see **Figure 5a**). Some more distant and massive clusters such as NGC 2477, NGC 2506, and NGC 6819 present a few tens of candidate RC stars in their CMDs (see Grocholski & Sarajedini 2002, Percival & Salaris 2003), although with uncertain memberships.

Even if they are few in open clusters, RC stars are critical in the determination of their distances and ages via isochrone fitting methods. Indeed, for a cluster of known metallicity, it is enough to fit the RC position in a CMD to almost completely determine its distance modulus and extinction values [as anticipated early on by Cannon (1970)]. Then, the next cluster parameter left to be adjusted is the cluster age, which can be determined by fitting the main sequence turnoff (MSTO). Because the RC position presents a modest variation with age, the process should ideally require a couple of iterations to ensure a consistent fit in all regions of the CMD.

Of course, this exercise makes sense only if the RC in the isochrones reproduce the RC in clusters of known distances. This cannot be checked in clusters with accurate *Hipparcos* parallaxes because all such objects are younger than 1 Gyr (van Leeuwen 2009). Percival & Salaris (2003) have compared the model predictions with the observed RC magnitude in clusters with empirical MS-fitting distances, finding they have excellent agreement with the Girardi & Salaris (2001) models within the error bars. The agreement does not hold for most evolutionary models in the literature, considering their wide variety of input physics and coverage of the mass-metallicity plan. In particular, models using the most updated input physics for the RGB phase tend to be systematically ~ 0.2 mag too bright compared to the data, as shown in **Figure 6**. This discrepancy can be reduced down to ~ 0.1 mag if the canonical Reimers (1975) mass loss with efficiency $\eta = 0.35$ (Renzini & Fusi Pecci 1988) is adopted in the models. Reasons for the variations between models of different input physics are discussed by Castellani et al. (2000).

Among the best-studied open clusters with good membership data, NGC 472 and NGC 7789 present an RC significantly more spread in luminosity than predicted by model isochrones (Mermilliod et al. 1998). These clusters are now suspected to host a dual RC (Girardi et al. 2000b). Because this feature is far clearer in the *Hubble Space Telescope* (HST) data of some intermediate-age Magellanic Cloud clusters, its discussion is postponed to Section 3.7.

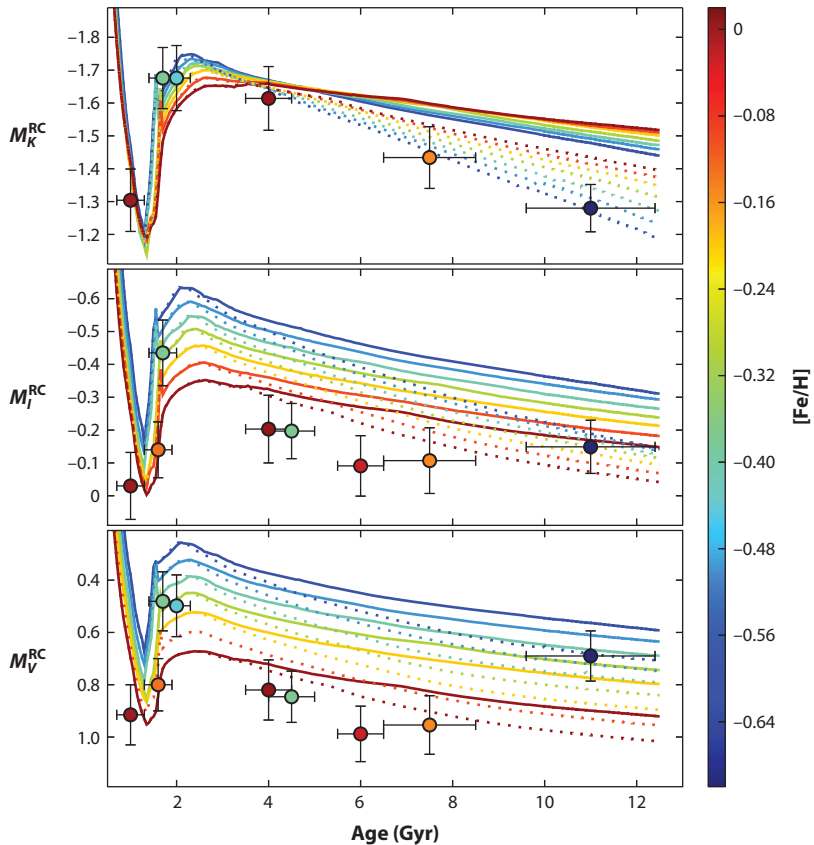


Figure 6

The red clump (RC) in open clusters of the Milky Way with, as much as possible, homogeneous derivation of distances [from main sequence (MS) fitting], and ages (from the MS turnoff), as presented by Percival & Salaris (2003). The sample also includes the old globular cluster 47 Tuc. For comparison, model predictions for metallicities between 0 and -0.5 dex are shown. Continuous lines are for models without mass loss on the first-ascent red giant branch, and dotted ones are for models assuming the Reimers (1975) mass loss with efficiency $\eta = 0.35$.

Another remarkable observation is that the difference between the median color of the RC and the RGB color at the same magnitude level correlates very well with age, at least for $B-R$ (Hatzidimitriou 1991). Such a relation is predicted by theoretical models, although they also predict a significant change in slope for solar and super-solar metallicities (Girardi 1999). Needless to say, *Gaia* parallaxes and revised membership probabilities will allow these relations to be tested and calibrated with much better accuracy.

3.2. The Solar Vicinity RC from *Hipparcos*

The CMD derived from *Hipparcos* parallaxes (Perryman et al. 1997) dramatically demonstrated that a large fraction of the nearby giants are in reality RC stars. Because the *Hipparcos* input catalog included virtually all stars with $V \lesssim 7$, and the typical parallax errors, σ_π , were of 1 mas (even after van Leeuwen 2007), a CMD limited to parallax errors $\sigma_\pi/\pi < 0.1$ (absolute magnitude

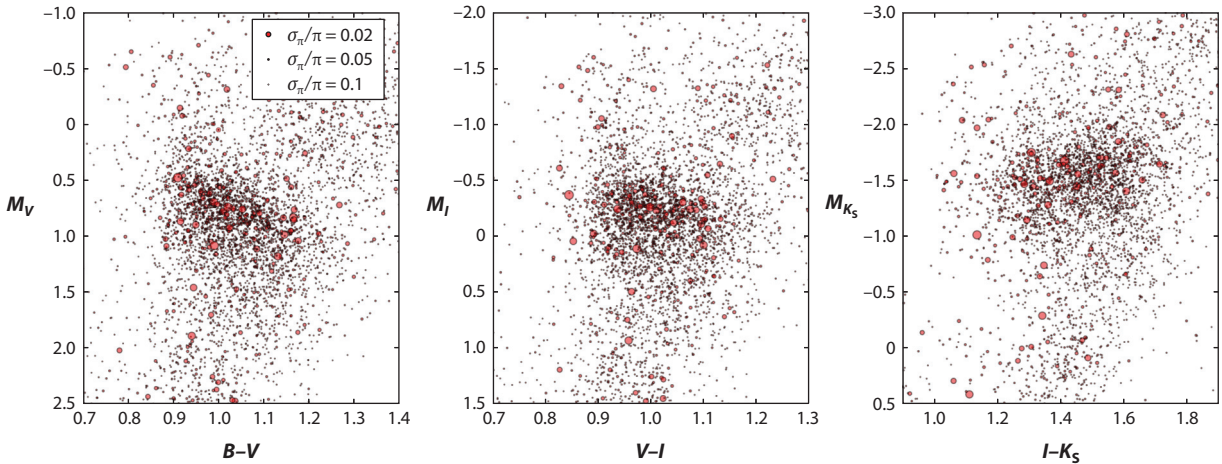


Figure 7

The Solar Neighborhood red clump revealed by *Hipparcos* in a few color-magnitude diagrams involving the Johnson-Cousins-2MASS B , V , I , and K_s filters. The photometry is taken from the Extended Hipparcos Compilation (Anderson & Francis 2012), with absolute magnitudes derived from van Leeuwen's (2007) revised parallaxes. The size of the data points scales inversely with the relative error in the parallax, so as to visually enhance the stars whose positions in the plot are more robust. Only stars with parallax errors σ_π/π smaller than 10% are plotted.

errors $\lesssim 0.22$ mag) is essentially complete up to a distance of 100 pc for all giants of $M_V < 2$. Among 844 of these giants in *Hipparcos*, 508 are candidate RC stars (with $0.5 < M_V < 1.5$ and $B-V > 0.8$). Theoretical simulations of this sample from Girardi et al. (2005) indicate that the genuine CHeB stars in this volume number nearly 390 and that they correspond to 31% of all red giants (comprising those at the bottom of the RGB).

Three different versions of the *Hipparcos*-derived CMDs are shown in **Figure 7**. The V versus $B-V$ version is the most reliable owing to the uniformity and accuracy of its photometry. The other CMDs, involving the I and K_s passbands, have been used often for distance-measurement arguments. It is evident from this plot (see Francis & Anderson 2014) that the RC mean slope in the CMD depends on the color-magnitude combination being plotted.

Paczynski & Stanek (1998) noted that their ~ 600 candidate RC stars with reliable VI photometry and $\sigma_\pi/\pi < 0.1$ have an I -band mean magnitude practically independent on the $V-I$ color. After correcting for a few minor effects, a Gaussian fit of its distribution produced a mean $M_I = -0.279 \pm 0.088$ mag, and a dispersion of about 0.23 mag. The small error in the mean M_I and the near constancy with color opened the way for the use of the RC as a standard candle, as we discuss below in Section 4.1. It also prompted the multiband photometry and spectroscopy of the *Hipparcos*-identified RC stars (e.g., Zhao et al. 2001, Valentini & Munari 2010, Laney et al. 2012) in order to identify correlations between RC intrinsic magnitudes and other stellar parameters.

Upon first inspection, the Solar Neighborhood RC is featureless but for a dispersion in color, which can be easily interpreted in terms of age and metallicity dispersions. However, comparison with synthetic models of the RC led Girardi et al. (1998) to identify the presence of an SRC at its faintest and bluest extreme. Indeed, the stars with the most accurate parallaxes in **Figure 7** seem to draw a second concentration at $M_V = 1$ mag and with $B-V$ between 0.9 and 1 mag. However, this feature is not that clear in the *Hipparcos* data, and the visual evidence can be substantially weakened by modifying the way the data are plotted. Nowadays, the strongest indication we have that this SRC feature in *Hipparcos* data is real—and represents a substantial fraction of the nearby

MACHO: Massive Compact Halo Object

OGLE: Optical Gravitational Lensing Experiment

RC stars—comes from independent data from *Kepler* (Section 3.5), which samples a much larger range in distances than does *Hipparcos*.

3.3. The RC in Wide-Area Photometric Surveys of the Milky Way

With so many RC stars observed in the Solar Neighborhood and in open clusters, it is obvious that they should also be a sizable fraction of the giants observed throughout the MW galaxy. That this is the case has been made evident in deep CMDs of the Bulge collected by the several phases of the Massive Compact Halo Object (MACHO) and Optical Gravitational Lensing Experiment (OGLE) surveys (Alcock et al. 1997, Popowski et al. 2005, Paczyński & Stanek 1998, Nataf et al. 2010), and more recently by the VVV (Saito et al. 2012, Minniti et al. 2014). All these surveys indicate a very well-populated RC elongated along the reddening vector. In relatively less-reddened areas of the Bulge such as Baade’s Window, the RC is observed at $I \simeq 14.4$ (Paczyński & Stanek 1998) or $K_s \sim 13$ (Saito et al. 2012).

The most detailed near-IR CMDs recently indicated a complicated pattern of double RCs along several Bulge lines of sight (McWilliam & Zoccali 2010, Nataf et al. 2010), with separations between the two RCs totalling up to 0.3 mag. VVV reveals that this RC splitting, absent in the Bulge center, becomes more pronounced in high Galactic longitudes in both hemispheres (Saito et al. 2011). The easiest interpretation of such a feature is in terms of populations at different distances, implying that we are seeing the X-shaped structure in the Bulge (Cao et al. 2013, Wegg & Gerhard 2013, Wegg et al. 2015, Nataf et al. 2015; see also Bland-Hawthorn & Gerhard 2016 in this volume). We note that the split RC in the Bulge is not related to the observation of a double RC in the bulge globular cluster Terzan 5 (Ferraro et al. 2009), which is best interpreted in terms of multiple populations formed in a formerly much more massive cluster (Massari et al. 2014).

In the general field of the MW, RC stars are at varying distances along the lines of sight, resulting in vertical features in the CMD rather than a well-defined clump. In the 2MASS and UKIDSS CMDs of the MW disk, the VS (**Figure 8a**) caused by the RC is well evident at $J-K_s \sim 0.75$ mag. It is sometimes blurred or inclined in lines of sight that have a strong differential extinction and might be confused with the VS found at $J-K_s = 0.85$ mag, which is caused by cool dwarfs of $M \lesssim 0.5 M_\odot$. We come back to this topic in Section 4.3.

3.4. The RC in Massive Spectroscopic Surveys

The spread of the RC in wide-area photometric surveys of the MW, due to both differential reddening and the wide range in distances, severely limits the possibility of building samples of RC stars free from other contaminants (mainly RGB stars). In large spectroscopic surveys, however, RC stars can be identified by their concentration in the effective temperature versus surface gravity plane, $T_{\text{eff}} \times \log g$. The intrinsic dispersion for a single-aged model RC is typically less than 0.1 dex in $\log g$ (as can be inferred from **Figure 3a**), and is confined to within 0.5 dex among RC stars of all ages and metallicities (**Figure 3c**). For the multiple populations in the MW disk, models such as those from Girardi et al. (2005) indicate an intrinsic $\log g$ dispersion of the order of 0.15 dex (1σ), which is less than the typical errors in the derivation of spectroscopic surface gravities.

Thanks to this concentration in the $T_{\text{eff}} \times \log g$ plot, large numbers of candidate RC stars have been identified among the targets of large spectroscopic surveys such as RAVE (Zwitter et al. 2010, Munari et al. 2014), Abundances and Radial Velocity Galactic Origins Survey (ARGOS) (Ness et al. 2013), and APOGEE (Bovy et al. 2014). An example taken from APOGEE is shown in **Figure 8**, where the RC concentration is evident. Obviously, any sample of RC stars selected from

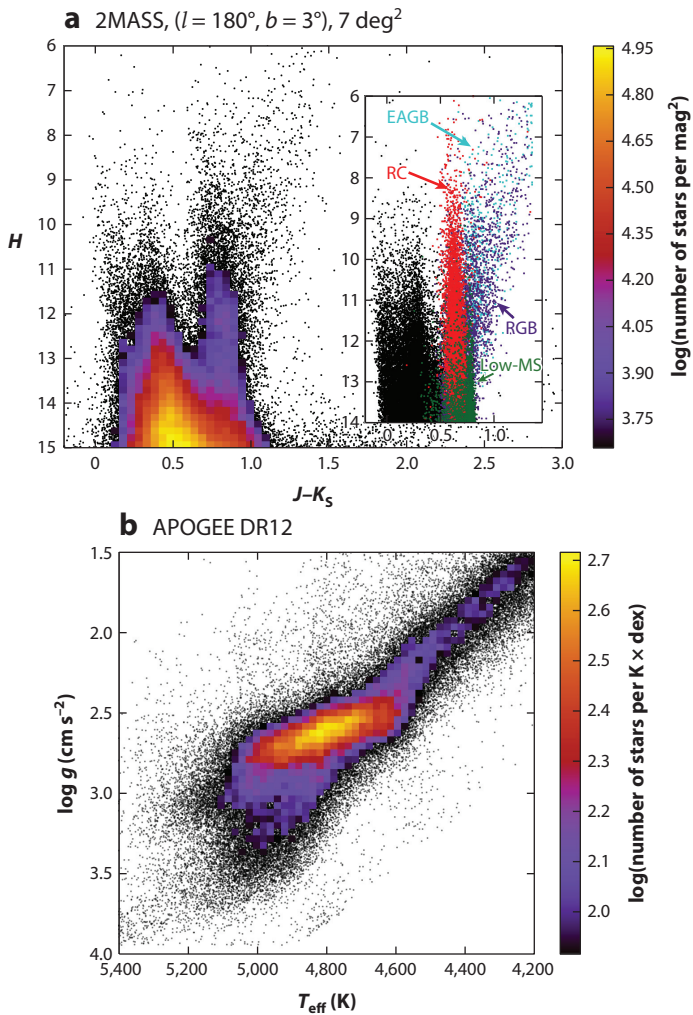


Figure 8

(a) The 2MASS color-magnitude diagram for a low-latitude field toward the outer Milky Way (MW), used in the target selection of APOGEE (figure based on Zasowski et al. 2013). The red clump (RC) vertical sequence is clearly evident at $J - K_s \simeq 0.75$ mag. The inset shows a simulation for the same field based on the TRILEGAL population model of the MW (Girardi et al. 2005), marking the RC and its main “contaminants” with different colors. This specific model adopts a simplified prescription for the dust distribution—namely an exponential layer with a scale height of 110 pc and a local A_V density of 0.75 mag kpc $^{-1}$ —and no photometric errors. (b) The $\log g \times T_{\text{eff}}$ plot from APOGEE data release 12 (DR12, Ahn et al. 2014). The bulk of observed stars have $H < 14$ and $(J - K_s)_0 > 0.5$ mag. Notice the large fraction of RC stars detected between $\log g = 2.4$ and 3.0. Abbreviations: EAGB, early asymptotic giant branch; low-MS, low-main sequence; RGB, first-ascent red giant branch.

this diagram will include some contamination from RGB stars. This contamination can be roughly estimated from the following: For 1-M $_\odot$ solar-metallicity stars at the approximate surface gravity of the RC, the RGB surface gravity increases at a rate of $\Delta \log g / \Delta \tau \simeq 1.8 \times 10^{-8}$ dex year $^{-1}$; this rate increases to 5×10^{-8} dex year $^{-1}$ for stars in the vicinity of M_{HeF} . The time $\Delta \tau$ needed to overcome a box size of $\Delta \log g = 0.5$ dex is then somewhere between ~ 1 and 2.2×10^7 years,

compared with the typical 10^8 -year lifetime of low-mass RC stars. Of course, the real ratio will be modified by many other factors, such as the possible presence of the RGB bump (with lifetimes of $\sim 10^7$ years) inside the selection box (especially at low metallicities), the mass distribution of the RC, and the presence of an SRC. An RGB contamination on the order of 30% times the $\log g$ box width in dex might be considered as typical.

In order to limit this contamination while building the APOGEE-RC catalog, Bovy et al. (2014) applied T_{eff} -dependent cuts to consider the systematic T_{eff} difference between the RGB and RC stars having similar metallicities. This correction is effective only if the T_{eff} difference (on the order of 200 K) is smaller than the random errors in T_{eff} , as is the case for APOGEE data. In addition, Bovy et al. (2014) eliminates the bluer SRC by using a metallicity-dependent color cut. Once “clean RC samples” are built, given their well-constrained distances, they can be used as kinematical and chemical probes (see Section 4.4).

3.5. The RC in Massive Asteroseismic Surveys

Since the CoRoT and *Kepler* space missions, asteroseismology has increased its impact in many fields of stellar astrophysics (Chaplin & Miglio 2013). With respect to RC stars, the developments are mainly of two kinds.

First, measurements of the basic asteroseismic parameters, the average large frequency separation, $\Delta\nu$, and the frequency of maximum power of the Gaussian-like modulation of the mode amplitude, ν_{max} , together with the T_{eff} from spectroscopy, now provide direct radius and mass determinations for thousands of giants, including several hundred RC stars. These determinations pass through the so-called scaling relations that express $\Delta\nu$ in terms of mean stellar density $\bar{\rho}$ and ν_{max} in terms of surface gravity and T_{eff} (Chaplin & Miglio 2013, and references therein):

$$\begin{aligned}\Delta\nu &\propto \bar{\rho}^{1/2} \propto M^{1/2} R^{-3/2}, \\ \nu_{\text{max}} &\propto g T_{\text{eff}}^{-1/2} \propto (M/R^2) T_{\text{eff}}^{-1/2}.\end{aligned}\quad (5)$$

The observed distributions of ν_{max} and $\Delta\nu$ have nicely revealed the peaks corresponding to the main body of the RC; for instance, for CoRoT the RC peaks at $\nu_{\text{max}} = 30.2 \pm 0.2 \mu\text{Hz}$ and $\Delta\nu = 3.96 \pm 0.33 \mu\text{Hz}$ (Miglio et al. 2009, Mosser et al. 2010), which correspond to the $\sim 10 R_{\odot}$ typical of RC stars. Importantly, $\log g$ determinations based on asteroseismic data are considered to be more reliable than those derived from spectroscopy alone (e.g., Pinsonneault et al. 2014), which opens the way to studies of the fine structure of the RC. Indeed, the SRC can now be clearly identified in the asteroseismic data. Its observation quickly improved from the first timid suggestions of its presence (Mosser et al. 2010, Kallinger et al. 2010) to more consistent evidence (Huber et al. 2010, Hekker et al. 2011), reaching finally the clear-as-day SRC display from Pinsonneault et al. (2014), shown in **Figure 9a**.

In the few star clusters observed by CoRoT and *Kepler*, the comparisons between the derived stellar parameters and theoretical isochrones promise to provide stringent constraints for models of RC stars. Suffice it to recall the case of NGC 6791, where the derivation of the mass of RC and RGB stars, via their $\Delta\nu$, ν_{max} , and T_{eff} plus scaling relations, allowed Miglio et al. (2012) to estimate the integrated mass loss (which presumably occurred close to the tip of the RGB), pointing to substantially less mass loss than was expected with the classical Reimers (1975) formula calibrated with globular clusters.

The other significant development from asteroseismology came from the discovery of the coupling between gravity waves in the dense radiative cores and the acoustic waves in the envelopes of red giants (Beck et al. 2011). Measurement of the so-called period spacing, ΔP (or its asymptotic version, $\Delta\Pi_1$), of these mixed modes provides a clear separation between RC and RGB stars of

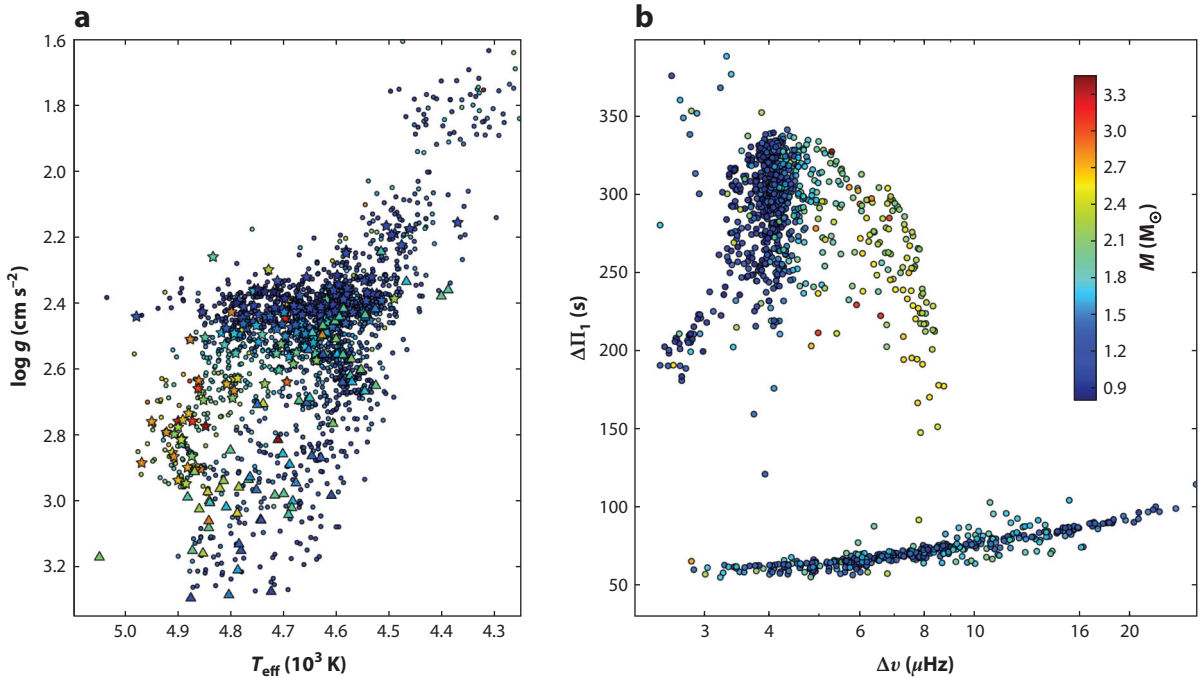


Figure 9

The new astroseismic views of the red clump (RC). (a) The *Kepler* stars from the APOKASC sample (Pinsonneault et al. 2014), placed in the classical T_{eff} versus $\log g$ plot but with $\log g$ derived from asteroseismic quantities plus scaling relations rather than from spectroscopy. Stars are color coded by the stellar mass M (cf. the scale in panel b). It is striking how the RC structure—and in particular the secondary red clump (SRC)—becomes well delineated in this plot, even if the observed stars are distributed over a very wide range of distances (see Rodrigues et al. 2014). Stars with observed $\Delta\Pi_1$ from Mosser et al. (2014) are marked as either RC (*stars*) or first-ascent red giant branch (RGB; *triangles*). (b) The $\Delta\Pi_1$ versus $\Delta\nu$ diagram from the *Kepler* giants examined by Mosser et al. (2014), again color coded by the stellar mass M . Errors in these quantities are typically of 5 s, 0.05 μHz , and $0.2 M_{\odot}$, respectively. The two groups of stars neatly separated in $\Delta\Pi_1$ correspond to core helium-burners (RC and SRC; for $\Delta\Pi_1 \gtrsim 120$ s) and RGB stars (for $\Delta\Pi_1 \lesssim 100$ s). Moreover, the SRC sequence stands out clearly at $\Delta\nu > 5 \mu\text{Hz}$, as it comprises CHeB stars that are more massive than $\sim 1.8 M_{\odot}$. All sequences are in the approximate locations predicted by evolutionary models (see Stello et al. 2013).

similar radii (Bedding et al. 2011, Mosser et al. 2011, 2014; Stello et al. 2013) (as illustrated in Figure 9b).

The $\Delta\Pi_1$ versus $\Delta\nu$ diagram is now becoming one of the most promising diagnostic plots for giants in the MW. As illustrated first by Bedding et al. (2011), Mosser et al. (2011), and Stello et al. (2013) (and later more clearly in Mosser et al. 2014), CHeB stars of low mass draw a compact sequence at $\Delta\nu < 5 \mu\text{Hz}$ and $\Delta\Pi_1 > 200$ s, which is well separated from the RGB and, in many respects, similar to the compact main RC seen in different CMDs. However, the asteroseismic data provide sufficient resolution to distinguish the mass sequence of these stars, as well as to draw their evolution toward larger $\Delta\Pi_1$ and, later, toward smaller $\Delta\nu$ (Mosser et al. 2014). Moreover, SRC stars with masses between $1.9 M_{\odot}$ and $2.4 M_{\odot}$ draw an appendix to the RC reaching $\Delta\nu = 9 \mu\text{Hz}$ and $\Delta\Pi_1$ close to 100 s; CHeB stars of higher masses, although rare in *Kepler* data, redistribute backward along the same sequence. Montalbán et al. (2013) show that the $\Delta\Pi_1$ along the SRC sequence traces the core mass at He ignition, hence allowing us to measure empirically the masses of stars that are just above M_{HeF} , which corresponds to measuring

the efficiency of convective overshooting during their MS. Complications in this method can arise from the metallicity spreads within the *Kepler* sample as well as from residual uncertainties in the scaling relations (Equation 5) that lead to the masses of RC stars (Miglio et al. 2013). However, it is reasonable to expect that improvements in the determination of asteroseismic parameters (compare Stello et al. 2013 with Mosser et al. 2014 to appreciate the quick progress regarding $\Delta\Pi_1$), added to more extensive spectroscopic observations (e.g., Pinsonneault et al. 2014) and a detailed calibration of scaling relations using stars in clusters, will soon allow us to derive definitive conclusions about overshooting from these data. Equally exciting—although probably more challenging—is the perspective of directly constraining the He content of RGB and RC stars from the “acoustic glitches” and their characteristic periodic signature in the frequencies of acoustic modes (Broomhall et al. 2014).

Measurements of $\Delta\Pi_1$ are not straightforward and are available for just a fraction of the *Kepler* and CoRoT samples. But this fraction is increasing. The $\log g$ versus T_{eff} versus mass diagram derived from the APOKASC catalog (Pinsonneault et al. 2014) shown in **Figure 9**, for instance, is being slowly complemented with period spacings, and with additional parameters derived from high-resolution spectroscopy, such as rotational velocities and chemical abundances. The importance of these additional parameters to further constrain stellar-evolution models is becoming evident; suffice it to mention the slowing down of rotation between RGB and RC stars detected by Mosser et al. (2012), or the unexpected identification of one lithium-rich giant in the *Kepler* field as being a $1.5\text{-}M_{\odot}$ RC star by Silva Aguirre et al. (2014). Interestingly, additional insights, $\log g$ estimates, and separation between RC and RGB stars may be provided by diagrams involving the “8-hr flicker,” i.e., the high-frequency variations (<8-h timescales) observed by *Kepler* (Bastien et al. 2013).

3.6. The RC in Other Local Group Galaxies

Although the RC has been observed in galaxies as far as in the Sculptor and M81 groups (e.g., Dalcanton et al. 2009), the farthest galaxies in which its fine CMD details are revealed by means of HST photometry are in the M31 subgroup (Williams et al. 2009, 2014; Monachesi et al. 2011) (see **Figure 10**). In the Local Group, all metal-poor dwarf galaxies containing intermediate-age populations host an RC in addition to the HB. Good examples are the Carina (Smecker-Hane et al. 1994), Leo I (Gallart et al. 1999), and Phoenix (Holtzman et al. 2000) dwarf spheroidals. The most metal-poor RC observed in good detail is probably in Leo P, with $[\text{Fe}/\text{H}] = -1.8$ (McQuinn et al. 2015).

For obvious reasons, the galaxies providing the most detailed and complete observations are the Magellanic Clouds, where the RC population was first revealed by a series of modest-scale optical surveys (Olszewski et al. 1996, Zaritsky & Lin 1997, Beaulieu & Sackett 1998, Bica et al. 1998, Piatti et al. 1999), by dozens of HST pointings (e.g., Holtzman et al. 1997, Ibata et al. 1998, Weisz et al. 2013), and then much more systematically by the OGLE surveys (Udalski 1998, Skowron et al. 2014), and partially by the Dark Energy Survey (Balbinot et al. 2015) and SMC in Time: Evolution of a Prototype (STEP) interacting dwarf galaxy (Ripepi et al. 2014). The InfraRed Survey Facility (Kato et al. 2007) provided the first extensive near-IR observations, with more detail being revealed by the much deeper (and ongoing) VISTA survey of the Magellanic Clouds (VMC) (Cioni et al. 2011).

Figure 10 shows some of these observations and compares them with a simple simulation. As can be appreciated, all the structures predicted by theoretical models have counterparts in the observations. For regions of low internal extinction, these observations usually reveal a compact main RC accompanied by an SRC, with widths generally small enough to be interpreted in terms

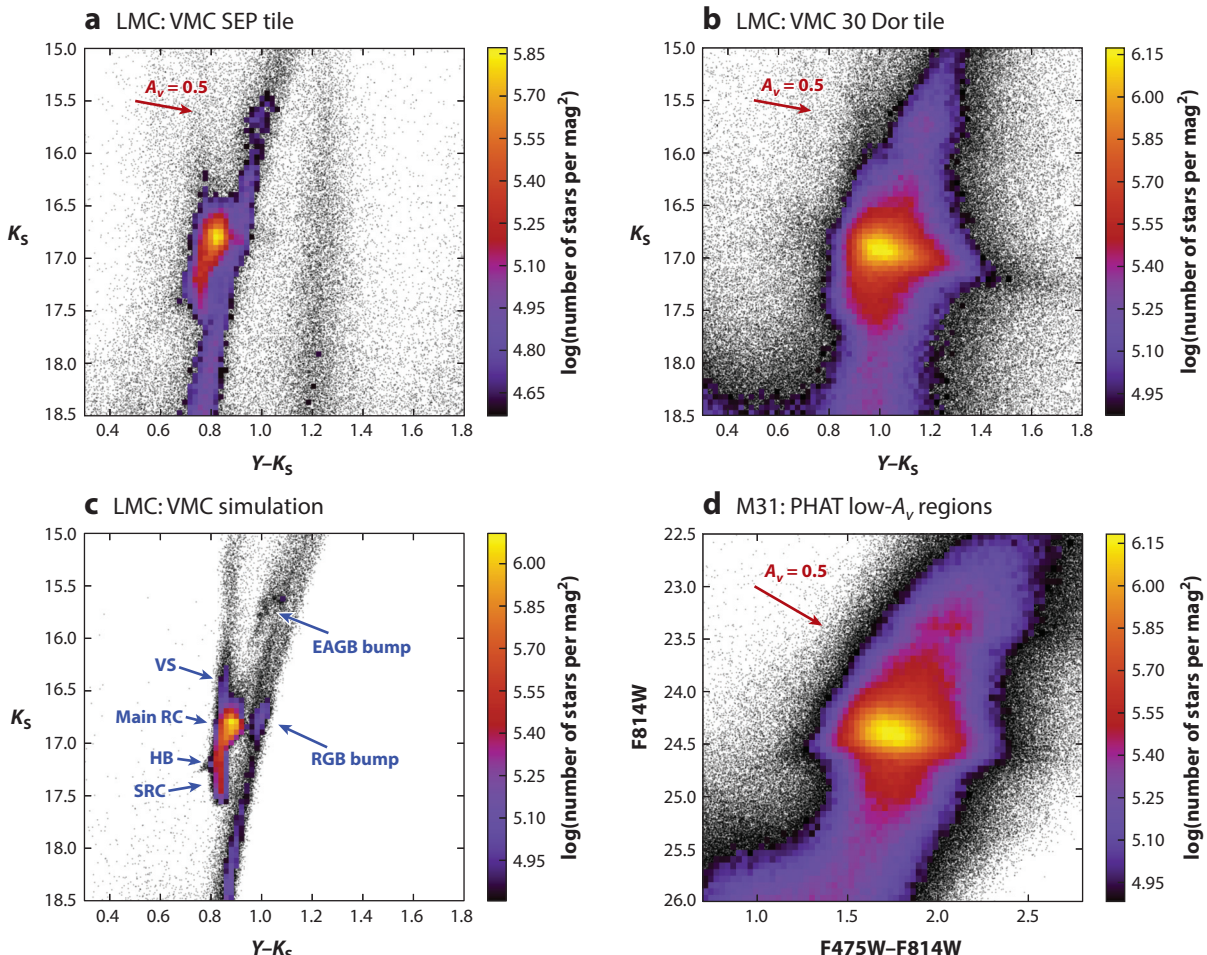


Figure 10

High-quality color-magnitude diagrams (CMDs) revealing the fine structure of the red clump (RC) in nearby galaxies. Panels *a* and *b* refer to the VISTA survey of the Magellanic Clouds (VMC) near-infrared CMDs of two different 1.6-deg 2 regions in the Large Magellanic Cloud (LMC) disk, namely (*a*) the region containing the South Ecliptic Pole located ~ 4.5 kpc to the northeast of the LMC center and (*b*) the highly extinguished and dense region around the 30 Dor nebula (see also Tatton et al. 2013). In both cases, the RC concentration contains about a third of all stars redder than $Y - K_s = 0.5$ mag and brighter than the first-ascent red giant branch (RGB) base at $K_s \sim 20$ mag (excluding the foreground Milky Way stars observed in the South Ecliptic Pole field at $Y - K_s \simeq 1.2$ mag). (*c*) A simple model for the LMC produced with the TRILEGAL code and PARSEC tracks (Girardi et al. 2005, Bressan et al. 2012) and the Holtzman et al. (1997) star-formation history, assuming null extinction, a distance of 50 kpc, and 0.01-mag photometric errors (1σ). The several CMD features recognizable around the RC are indicated. (*d*) The RC of low-reddening regions in the M31 disk, selected from the Panchromatic Hubble Andromeda Treasury (PHAT) catalog (Williams et al. 2014). The arrows indicate the reddening vector corresponding to $A_v = 0.5$ mag of interstellar extinction. In all panels, a Hess diagram with a logarithmic color scale is used in CMD regions where the dots would saturate the image. Abbreviations: EAGB, early asymptotic giant branch; HB, horizontal branch; SRC, secondary red clump; VS, vertical structure.

of a mixture of populations of different ages and metallicities (e.g., Girardi 1999). This is clearly the case for the outer Large Magellanic Cloud (LMC) disk (South Ecliptic Pole field in **Figure 10**), which in addition to the SRC presents clear signs of a VS and HB stars. In denser LMC regions like that around 30 Dor, the RC has essentially the same structure, but it also has additional broadening due to differential extinction.

A single value of distance modulus suffices to interpret most of the RC observations in nearby galaxies. There are, however, recurrent claims of depth structures being detected in several points across the Clouds, based on the RC magnitude width and following the method designed in the classical work by Gardiner & Hawkins (1991). The method assumes that the excess dispersion, σ_{geo} , with respect to a reference value, σ_{int} —derived in regions with well-characterized reddening and photometric errors, σ_{err} —can be assigned to depth structures inside the Clouds, i.e.:

$$\sigma_{\text{geo}}^2 = \sigma_{\text{total}}^2 - (\sigma_{\text{int}}^2 + \sigma_{\text{err}}^2). \quad (6)$$

For the SMC, 2σ depths exceeding 12 kpc were initially found, especially in its eastern regions (Gardiner & Hawkins 1991, Gardiner & Hatzidimitriou 1992). The intrinsic dispersion caused by stellar ages and metallicities can be partially responsible for such large derived SMC depths, as recognized by Girardi (1999) and Subramaniam & Subramanian (2009, 2012). Nowadays, claims of large SMC depths are far more substantiated in the eastern Wing of the SMC, where the RC widens and even splits into both a bright feature and a faint feature (Nidever et al. 2013), with width/separation clearly in excess with respect to the spreads that could be explained by population effects.

Finally, **Figure 10** shows the situation for low-extincted regions in the outskirts of M31, from the Panchromatic Hubble Andromeda Treasury (Dalcanton et al. 2012), which probably represents the best possible view of the RC in spirals up to now. As can be seen in the figure, the VS of the M31 RC resembles the one in the LMC. However, these observations present a significant color spread that does not follow the reddening vector and, hence, cannot be simply interpreted in terms of differential extinction. A significant dispersion in metallicity is likely associated with it as well.

3.7. The RC in Star Clusters of the Magellanic Clouds

Star clusters in the Magellanic Clouds present a special case because of three aspects: their well-constrained values for distances and foreground extinction, their large stellar numbers (both absolute and relative to their surrounding fields) compared to open clusters in the MW, and the presence of high-quality HST observations.

The assumption that cluster distances (and to a lesser extent the extinctions) were the same for all clusters in either the LMC or SMC has long since allowed tests of the basic behavior of the RC luminosity with age, as well as allowed us to follow the development of the RGB. Corsi et al. (1994) first detected the minimum RC luminosity that occurs at ages $t \sim t_{\text{HeF}}$ —coinciding with the LMC cluster NGC 2209—in BV passbands. The flattening of the luminosities at older ages is also apparent in the same data, despite the low number of such clusters in their sample. A subsample of these clusters were observed in the near-IR by Ferraro et al. (2004); they identified the marked increase in the number ratio between RGB and RC stars, $N_{\text{RGB}}/N_{\text{RC}}$, that follows the transition at t_{HeF} , but they were essentially unable to assign an absolute age to this transition.

A similar survey of RC photometry has been accomplished in near-IR passbands by Grocholski et al. (2007), who used the behavior of the RC in the models to derive individual cluster distances, confirming that the clusters follow the same disk geometry as that in the LMC field. As for the

SMC, Crowl et al. (2001) finds evidence of a significant depth using a sample of clusters with RC-based distances.

There is ample room to improve these analyses with the aid of deeper near-IR and HST photometry. Indeed, the high-quality HST observations accumulated in the past ten years have proven very important for testing the predictions regarding the structure of the RC, especially for the most populous clusters. First, they have confirmed that the RC is significantly more elongated in young clusters, as opposed to compact RCs observed at ages of >2 Gyr. This observation perfectly fits with the general scenario that predicts a marked transition in the RC shape between clusters before and after t_{HeF} (see Section 2.1 and **Figure 5d**). Much more surprising was the observation that there are single clusters containing both an elongated and a compact RC. These cases appear in the form of a compact RC plus a downward extension—the SRC—that resembles the structures observed in the fields of galaxies. The most striking example is NGC 419 in the SMC, whose core presents a marked RC with 341 stars, plus 47 stars in the SRC (Girardi et al. 2009). If we consider that the upper part of the SRC is actually mixed in the CMD among the main RC stars, the ratio between CHeBs with different evolutionary histories is actually larger than implied by this simple count ratio. **Figure 11** presents the CMD of this cluster, together with its “classical” interpretation in terms of a cluster containing a significant spread in ages.

As suggested by Girardi et al. (2009) and confirmed by Goudfrooij et al. (2014), dual RCs are actually present in many of the populous intermediate-age Magellanic Cloud clusters, like NGC 1751, NGC 1783, NGC 1806, NGC 1846, NGC 1852, and NGC 1917, all of them having MSTO ages close to the t_{HeF} limit in which the dichotomy is expected to appear. Moreover, they all display impressive extended main sequence turnoffs (eMSTOs). It is natural to associate the two phenomena, assuming that the same effect that causes stars to spread along the MSTO also causes the small spread in core mass after the MS, which is necessary to create dual RCs. However, there is no consensus yet on the cause of eMSTOs; the leading interpretations are linked to either an age dispersion inside the clusters (Goudfrooij et al. 2011, 2014, Girardi et al. 2011) or a spread in rotational velocities among coeval stars (Bastian & de Mink 2009, Brandt & Huang 2015).

Interestingly, the dual RCs also influence this discussion. As observed by Goudfrooij et al. (2014), in all clusters in which a dual RC has been observed, the fraction of RC stars in the SRC strongly correlates with the fraction of MSTO stars in the bluest section of the eMSTOs. This observation is consistent with the interpretation that the bluest section of the eMSTOs is actually populated by stars of higher initial masses and, hence, younger than the cluster mean age. It practically rules out Bastian & de Mink (2009)’s interpretation that the blue eMSTOs correspond to slow rotators because slow rotators are expected to have smaller core masses after the MS (Eggenberger et al. 2010) and evolve to the main RC rather than to the SRC. Claims that the observed RC is too compact to derive from populations with a significant age spread (Bastian & Niederhofer 2015) have been disputed on the basis of stellar models computed with a better mass resolution (Goudfrooij et al. 2015). However, an alternative rotation-spread scenario has been recently proposed by Brandt & Huang (2015), who indicate that the bluest part of eMSTOs is populated by fast rotators observed nearly face-on rather than by the nonrotators indicated by Bastian & de Mink (2009). If these fast rotators produce the largest core masses at the end of the MS, as expected, hence barely escaping the development of electron degeneracy, the correlation with the SRC would be naturally explained. Overall, this is still an ongoing discussion, and, needless to say, it bears somewhat on the interpretation of multiple features observed in the much older MW globular clusters.

Irrespective of the causes of eMSTOs, the presence of dual RCs in single clusters brings the possibility of directly probing the mass limit M_{HeF} and, hence, of setting stringent limits on mixing processes during the MS—as with, for instance, convective overshooting (Girardi et al. 2009). The

eMSTO: extended
main sequence turnoff

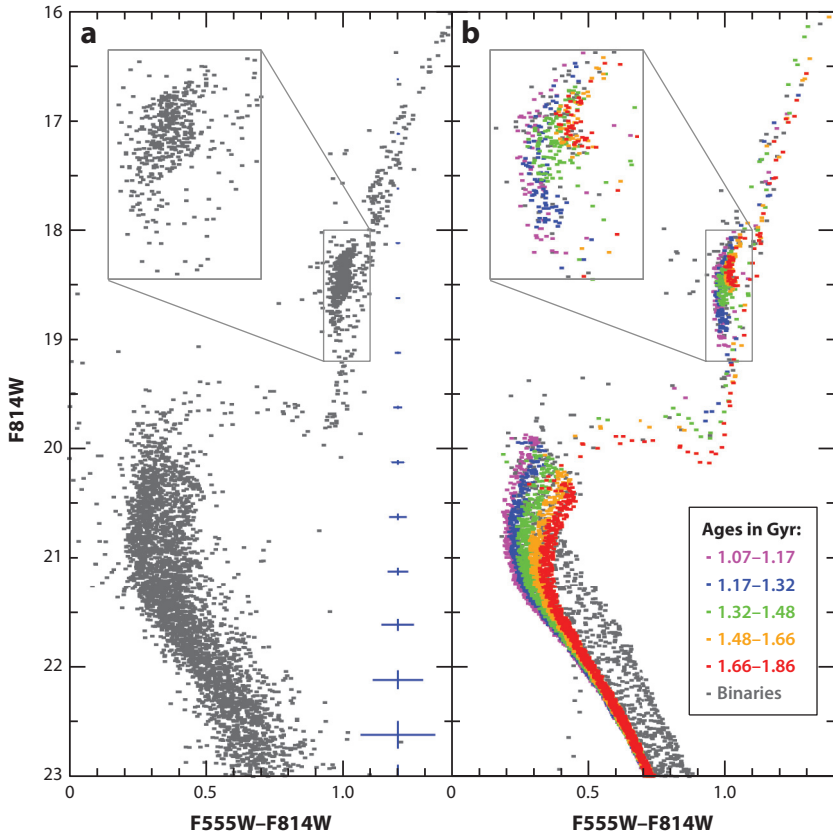


Figure 11

(a) The *Hubble Space Telescope* color-magnitude diagram for the Small Magellanic Cloud star cluster NGC 419 (Girardi et al. 2009), with the evident presence of both an extended main sequence turnoff and a dual red clump. (b) A model (based on Girardi et al. 2013) suggesting the easiest explanation for both features: a significant spread in stellar ages. Apparent binaries contribute to the spread along the main sequence.

main point is that these clusters have, undoubtedly, turnoff masses around the M_{HeF} limit, which depends on the amount of core overshooting. The MSTO to RC mean color separation is a good proxy for the turnoff mass. Thus, such clusters allow us to access simultaneously the turnoff mass and M_{HeF} from the joint use of the mean eMSTO–RC separation and the RC morphology. Girardi et al. (2009) applied this idea to NGC 419 and demonstrated that models with moderate overshooting, together with an age of 1.35 Gyr, provide the best simultaneous fit in this cluster. Importantly, classical models following the Schwarzschild criterion for convective borders are simply ruled out by this method. By contrast, if a spread in rotation turns out to be a determinant for the formation of eMSTOs and dual RCs, just the final interpretation of this result would change, replacing the measurement of a “mean efficiency of convective overshooting” with the measurement of a “mean efficiency of core growth due to both overshooting and rotational mixing.”

4. REMARKS ABOUT POPULAR RC METHODS

As discussed above, RC stars occupy a narrow region of the CMD of nearby galaxies and star clusters. Under the assumption that the RC is always the same—or at least changes in a smooth

and predictable way—among different populations, we can look for its magnitude and color distributions to map these populations in distance and reddening. This is the basis of all “red clump methods,” which we discuss in the following section.

4.1. RC Stars as Standard Candles

The history of the use of the RC as a distance indicator starts with the work by Cannon (1970) and is well substantiated by almost every work on stellar evolution in which the CHeB phase of low-mass stars has been computed. These works indicated clearly that they should have more or less the same core mass and, hence, luminosity. In order to transform the RC from a “promising distance indicator” to a “standard candle,” the only missing piece of information was a reliable calibration for its absolute magnitude. Indeed, the theoretical calibrations clearly suffered from all the uncertainties in the RGB evolution, most notably in the plasma neutrino losses, electron conduction, opacities, and equation of state (e.g., Castellani et al. 2000), which were causing uncertainties of $\sim 0.01 M_{\odot}$ in the core masses at He ignition and, hence, several hundredths of a magnitude in the brightness of ZACHeB stars.

This sorely missed absolute magnitude reference was finally provided by the accurate parallaxes from *Hipparcos*. Paczyński & Stanek (1998) set the basic method for empirically measuring this magnitude. First they built the luminosity function (LF) of all stars with parallax errors smaller than 10% (corresponding to 0.22-mag errors in absolute magnitudes), then fitted a function of the form

$$N(\lambda) = a + bM_{\lambda} + cM_{\lambda}^2 + d \exp\left[-\frac{(M_{\lambda}^{\text{RC}} - M_{\lambda})^2}{2\sigma_{\lambda}^2}\right], \quad (7)$$

where λ stands for a given passband (the I -band in the original method). The second-order polynomial in this equation represents the “background” of RGB stars and is sometimes replaced by power laws (Stanek et al. 1997) or exponentials (Nataf et al. 2015). The last term represents the RC distribution as a Gaussian of mean M_{λ}^{RC} and width σ_{λ} . Then, all one needs to do in an extragalactic system is to apply the same method to fit its apparent RC mean magnitude, m_{λ}^{RC} . The distance modulus $\mu_0 = 5 \log d - 5$ simply follows from

$$\mu_0 = m_{\lambda}^{\text{RC}} - M_{\lambda}^{\text{RC}} - A_{\lambda} + \Delta M_{\lambda}^{\text{RC}}. \quad (8)$$

The last two terms of Equation 8 stand for the interstellar extinction A_{λ} (which is practically null for the *Hipparcos* sample, at least for wavelengths longward of the I -band), and a possible “population correction,” $\Delta M_{\lambda}^{\text{RC}}$, which we include for completeness (see below) but was absent from the original method.

The caveats in the method are of three different types, associated with the following questions.

4.1.1. Does Equation 7 provide a reliable measurement of the RC mean magnitude? The fits to the data obtained with Equation 7 are excellent in nearly all cases in which RC distances have been computed. However, this is no surprise—in most cases the dispersion in the RC magnitudes was comparable with the photometric measurement errors. The same applies to the original *Hipparcos* data from Perryman et al. (1997), which, if limited to $< 10\%$ parallax errors, already ensures a width of about 0.15 mag to the RC (Girardi et al. 1998).

Additional spread comes from the fact that the RC has an intrinsic width due to stellar evolution, and—more importantly—it is not symmetric around its mean; even for the most simple case of a single-age, single-metallicity RC, the LF distribution is expected to be skewed toward the brighter magnitudes owing to the faster evolution in $\log L$ toward the end of the CHeB phase (Figure 3a). In the case where all possible ages are present in the observed populations, additional LF tails are expected from the SRC, VS, and HB substructures. Moreover, it is remarkable that another sharp

LF feature—the RGB bump—may be intervening at about the same magnitude level of the RC and contributing to the Gaussian “RC signal” as well (see **Figure 10**).

In principle, all of these shortcomings could be avoided by fitting population models to the observed LF instead of simple second-order polynomials plus Gaussians. Population models can easily be degraded to the observational conditions by applying the distribution of observational errors—e.g., those obtained by means of artificial star tests. This procedure clearly goes against the idea of simplicity that stands on the design of extragalactic standard candles. The first examples of this more elaborate modeling of the RC LF have begun to appear. For instance, in their study of the X-shaped bulge, Wegg & Gerhard (2013) adopt a model LF that, although fitted with a Gaussian, includes the skewness effect and also considers the RGB bump expected from the models.

4.1.2. How independent are the $M_{\lambda,0}^{\text{RC}}$ of the observed population? From a standard candle, one expects minimum deviations from the hypothesis of “constancy throughout the universe”; or at least one expects that the existing deviations are predictable as a simple function of other stellar observables—like the colors, pulsation periods, and metallicities. Perhaps no other distance indicator provides better evidence of this expectation than the RC.

One of the most striking conclusions in the seminal Paczyński & Stanek (1998) paper was that the observed RC mean magnitude in the I -band, for both the *Hipparcos* sample and the Bulge (Baade’s Window), was observed to be the same, within the uncertainties, for different bins of $V - I$ color. The color distributions between these two samples even present a significant overlap, which was interpreted as an overlap in the metallicity range and taken as evidence for a general independence of $M_{I,0}^{\text{RC}}$ on the population color and metallicity.

That idea, however, has not survived confrontation with new evidence. The approximation of “constancy with color” leads to an LMC distance that is 15% shorter than the values commonly assumed to date (Udalski 1998, Stanek et al. 1998). This prompted the introduction of theoretical population effects, $\Delta M_{\lambda}^{\text{RC}}$, in Equation 8 by Cole (1998), Girardi et al. (1998), Girardi (1999), and Girardi & Salaris (2001). This term represents the mean effect, on the RC mean absolute magnitudes, of all the differences in the distributions of ages and metallicities between the external galaxies and the *Hipparcos* sample. Because they depend on quantities (ages and metallicities) that are not easily derived from the RC photometry alone, they have to be computed with the aid of theoretical models of stellar populations.

For the *Hipparcos*–LMC system, these theoretically predicted corrections amounted to about 0.2 to 0.3 mag (Cole 1998, Girardi et al. 1998, Girardi & Salaris 2001) in the I -band, hence reconciling the LMC distance with the “classical” values of about 50 kpc. Because both the *Hipparcos* sample and the LMC contain populations of all ages from very young to very old, much of this correction comes simply from the average metallicity of these galaxy environments differing by about 0.4 dex.

Without entering into the details of the theoretical predictions—which in any case depend somewhat on uncertain relations like the SFRs and AMRs of both the Solar Neighborhood and LMC, and on the adopted set of stellar models—let us just quickly point out why a population correction is necessary even if the RC in the LMC and in the *Hipparcos* samples appear nearly horizontal in their respective I versus $V - I$ CMDs (see Girardi & Salaris 2001 for more details). The dependence of M_I^{RC} on age and metallicity is substantially different, as is shown in **Figure 3b** (and in a different way in **Figure 5b**). The total color-magnitude intervals of the observed RC stars will be defined by the AMR in the observed galaxy. In the Solar Neighborhood, the metallicities have changed little over many gigayears, so one can take a slowly decreasing line at the [M/H] versus age plot shown in **Figure 5b** and notice that the M_I^{RC} changes very little, at least for ages between 2 and 8 Gyr; this situation is likely to produce a nearly horizontal RC in the CMD.

For the LMC, a similar situation can be found, but it is for an age-metallicity line systematically shifted downward by about -0.4 dex; again the likely result is a nearly horizontal RC but with the systematic shift in metallicity producing an offset of about 0.3 mag between the LMC and the Solar Neighborhood. The quantitative details will depend on the SFR of the two galaxies and can only be found with detailed population synthesis models. Such models can explain the RC I -band magnitude being nearly constant with $V - I$ when measured internally to the LMC and the Solar Neighborhood and, at the same time, having a significant zero-point difference between these systems (Girardi & Salaris 2001).

Nowadays, the presence of significant population effects in the I -band is well documented (e.g., Alves et al. 2002, Percival & Salaris 2003) and widely accepted (see Pietrzyński et al. 2010).

4.1.3. Which wavelength/passbands minimize the population effects? Given that population effects are not marginal, one might wonder if there is a particular passband that minimizes its impact on distance determinations. Of course there is, but because the age and metallicity effects are not parallel (**Figure 3b**), there will not be a single wavelength that will minimize population effects for all observed populations and galaxies. In other words, there is no single M_{λ}^{RC} versus age, M_{λ}^{RC} versus $[\text{Fe}/\text{H}]$, or M_{λ}^{RC} versus color relation able to capture the entire intrinsic variation of this quantity.

Salaris & Girardi (2002) demonstrate that the use of the K -band minimizes the theoretically derived population effects for the *Hipparcos*–LMC–SMC cases, as previously suggested by Alves (2000). This is mainly because it greatly reduces the metallicity variations in the RC magnitude, as shown in the constant M_{K_s} lines running nearly parallel to the metallicity sequence in (**Figure 3c**). As an additional bonus, the use of the K -band reduces the impact of uncertainties in the mean extinction in Equation 8. These observations prompted the progressive move from the I -band RC method by Paczyński & Stanek (1998) to a near-IR one (e.g., Nishiyama et al. 2006).

Attempts to identify wavelengths in which population effects are minimized were followed by a few recalibrations of the absolute magnitude from *Hipparcos* in passbands redder than I , which in some cases implied redoing the photometry for bright stars, as done by Laney et al. (2012). A brief summary of these recalibrations is provided in **Table 1**. Most of these works are characterized by great concern in dealing with even minor corrections, like, for instance, the incompleteness, Lutz-Kelker (Girardi et al. 1998) and Trumpler-Weaver (Francis & Anderson 2014) biases. In addition, the revised *Hipparcos* parallaxes from van Leeuwen (2007) were adopted in 2008 (Groenewegen 2008). Even if non-null, these corrections cause just minor changes in the calibrations, at the level of a few hundredths of a magnitude. Even the ~ 0.1 -mag differences between peak and mean magnitudes (Francis & Anderson 2014) appear more relevant.

Given the fact that population effects at a level of several hundredths of a magnitude might still exist in any passband, all these efforts do not suffice to transform the RC into an accurate standard candle. Their merits are simply in reducing the already small systematic errors in RC distance determinations yet they fail to introduce any conceptual improvement in its straightforward application of Equations 7 and 8. Perhaps the more interesting variation into this scheme was the multiband approach introduced by Alves (2000). In short, he used VIK bands simultaneously to derive both the distance and extinction in the Bulge using a subsample of *Hipparcos* and Bulge stars with approximately the same spectroscopic metallicities and the assumption that such stars have the same intrinsic colors. This method in practice averages the RC distances, and their possible offsets, in all passbands. For the LMC, the same method (Alves et al. 2002) produces consistent evidence for the important population effects in the I -band, because setting ΔM_I to null produces the unphysical result of negative extinction.

Table 1 Determinations of mean red clump (RC) magnitude M_{λ}^{RC} , generally from *Hipparcos*

λ	M_{λ}^{RC}	Reference	Comments
<i>I</i>	-0.279 ± 0.088	Paczyński & Stanek (1998)	Includes reddening correction
<i>I</i>	-0.23 ± 0.03	Stanek & Garnavich (1998)	Volume limited to 70 pc
<i>I</i>	-0.209	Girardi et al. (1998)	Lutz-Kelker bias corrected
<i>I</i>	-0.22 ± 0.03	Groenewegen (2008)	First uses revised <i>Hipparcos</i> parallaxes
<i>I</i>	-0.24 ± 0.01	Francis & Anderson (2014)	Peak of luminosity distribution
<i>K</i>	-1.60 ± 0.03	Alves (2000)	First near-IR value
<i>K</i>	-1.62 ± 0.02	Grocholski & Sarajedini (2002)	Median from WYIN open clusters
<i>K</i>	-1.57 ± 0.05	van Helshoecht & Groenewegen (2007)	From 2MASS data on 24 open clusters
<i>K</i>	-1.54 ± 0.04	Groenewegen (2008)	First uses revised <i>Hipparcos</i> parallaxes
<i>K</i>	-1.613 ± 0.015	Laney et al. (2012)	New near-IR photometry for bright stars
<i>K</i>	-1.53 ± 0.01	Francis & Anderson (2014)	Peak of luminosity distribution
<i>J</i>	-0.984 ± 0.014	Laney et al. (2012)	
<i>H</i>	-1.490 ± 0.015	Laney et al. (2012)	
W1	-1.635 ± 0.026	Yaz Gökçe et al. (2013)	First mid-IR value
W2	-1.606 ± 0.024	Yaz Gökçe et al. (2013)	
W3	-0.028 ± 0.001	Yaz Gökçe et al. (2013)	

4.2. RC Stars as Extinction Probes

In order to estimate mean extinctions across a galaxy, all that is needed is a population of stars that can be easily identified in the CMD and assumed to be intrinsically homogeneous; their color-magnitude spread then can be attributed to variable extinction only. At first sight, the RC nicely meets these requirements.

Methods for using the RC as an extinction probe date back to Woźniak & Stanek (1996) and Stanek (1996) and utilize OGLE data for the MW Bulge. Another favorable situation for extinction measurements is met in the disk(s) of external galaxies, where the entire RC—and also the RGB—is observed to spread in the direction of the reddening vector. This is very clearly the case illustrated in **Figure 10** for the LMC 30 Dor region. Tatton et al. (2013) derive a detailed extinction map for this region by measuring the amount of the redward spread of the RC in VMC data. The same kind of dust mapping has been done extensively across both Magellanic Clouds using data from OGLE-III by Subramaniam (2005), Subramaniam & Subramanian (2009), and Haschke et al. (2011).

The RC has also been cleverly used to derive the extinction coefficients toward the MW Bulge (Nataf et al. 2013) and the 30 Dor region (De Marchi et al. 2014), and to derive the near-IR extinction curve by Nishiyama et al. (2009). The method makes use of several reddening vectors, involving observations in several filters, to reveal the shape of the extinction curve, as illustrated in De Marchi et al. (2014).

These extinction-mapping methods assume there is no systematic variation in the intrinsic RC properties across the observed area and along the line of sight. Large-scale extinction maps of galaxies with significant age and metallicity gradients (e.g., M31 and M33) would require a network of low-reddening regions for calibration. Even the wide-area extinction maps of the Magellanic Clouds (e.g., Haschke et al. 2011) might be affected by the systematic changes in the RC intrinsic color to some extent, given the evidence for systematic gradients in the intermediate-age and old populations across these galaxies (e.g., Balbinot et al. 2015).

In the old MW Bulge, the approximation that the RC has the same intrinsic properties is more reliable, at least on the small scales (fractions of degrees) for which extinction mapping is useful. Extended extinction maps of the MW Bulge have been provided by Gonzalez et al. (2011) and Wegg & Gerhard (2013) based on VVV data.

4.3. RC Stars as Density Probes

For the same reasons that RC stars have been used to probe mean distances and extinctions in external galaxies, they can also be used to probe the distribution of distances within the MW along particular lines of sight. The method has been specifically developed to take advantage of the large photometric databases in the near-IR, in particular 2MASS. Its rationale can be found in López-Corredoira et al. (2002). Essentially, one needs to identify on the $J - K_s$ versus K_s CMD the near-vertical locus created by RC stars observed at increasing distance moduli and extinctions and then convert the luminosities of these candidate RC stars in this locus into linear distances r by applying $r = 10^{K_s - M_{K_s} + 5 - A_{K_s}(r)}$, where M_{K_s} is the intrinsic RC magnitude derived from the *Hipparcos* sample. The extinction along the line of sight, $A_{K_s}(r)$, can be constrained by the way the RC locus becomes redder at fainter magnitudes, e.g., by using $A_{K_s} = 0.657 E(J - K_s)$. Then, the stellar density as a function of distance, $D(r)$, follows from the LF along the RC locus, $A(m)$, from

$$D(r) = \frac{A(m) \delta m}{\omega r^2 \delta r}, \quad (9)$$

where ω is the observed solid angle. With some variations, similar methods have been extensively used to probe the Bulge structure (López-Corredoira et al. 2007, Wegg & Gerhard 2013) and the disk warp and flare (López-Corredoira 2006, Cabrera-Lavers et al. 2008).

Some concerns with this method include the following: (a) the strong contamination of the RC locus at $J - K_s = 0.75$ by the RGB (and RGB bump) stars, whose distances will be overestimated in Equation 9. This obviously causes a blurring in the derived distance distributions; however, numerical experiments by López-Corredoira et al. (2002) show that the derived disk scale lengths are not significantly in error. Moreover, the method as applied to the Bulge by Wegg & Gerhard (2013) implements an iterative approach that takes into consideration the expected position of the RGB bump and its effect in the observed LF. (b) The possible contamination by intervening nearby dwarfs, whose “kink” at the bottom of the MS at $J - K_s = 0.85$ mag (Sarajedini et al. 2009) also causes a vertical strip in the CMD of MW fields, which is disturbingly close in color to the RC locus and more prominent than it at both high galactic latitudes or faint magnitudes (at $K_s > 13$; cf. López-Corredoira et al. 2002, and see also **Figure 8a**). These contaminants indicate that the RC method should be used only in samples dominated by giants, i.e., only for bright magnitudes and toward the MW Galactic Plane and Bulge.

The difficulties in defining a clean sample of RC stars for density estimation are more evident when it comes to estimating the structure of the outer MW Galaxy. In some cases, the identification of the RC stars in the CMD is far from being clear given the high level of contamination by stars located in front of the structures that are targeted for probing. For instance, the putative Canis Major galaxy was traced by RC stars by Bellazzini et al. (2006; see, however, López-Corredoira et al. 2007); in this case the RC appears as a modest and fuzzy bump in color-luminosity space whose identification is helped by a comparison with a “reference CMD” provided by a popular and well-behaved population model of the MW (namely the Besançon model by Robin et al. 2003). As another example, the maximum extent of the MW disk has been probed using candidate RC stars in VVV by Minniti et al. (2011). In this case, the RC is not even seen in the CMDs; what is detected

is just the luminosity level at which the stellar number density drops along different lines of sight, presumably by reaching RC stars located at the edge of the stellar disk. Needless to say, these are extreme cases for which we might still see significant changes in the quantitative results of RC density-estimation methods as better analysis tools and simulations of the intervening populations (and their line-of-sight structures) are developed.

Somewhat more subtle are the problems caused by population effects among RC stars themselves, including (*c*) the preferential sampling of populations of relatively young ages (1 to 4 Gyr) in the RC feature. Indeed, any age gradient present along the line of sight will cause a failure in the basic assumption behind Equation 9—namely that the observed number of RC stars is proportional only to the stellar density (taking out the geometric factors). Finally, (*d*) the assumption that the variation in the mean RC color with magnitude traces the increase in reddening with distance may fail, because age and metallicity variations also affect the RC mean color. For instance, the *Hipparcos* RC as observed by Laney et al. (2012) has an intrinsic width of about 0.2 mag in $J - K_s$ (from 0.55 to 0.75 mag), which can only be attributed to spreads in age and metallicity and which would be mistaken by a spread of 0.13 mag in A_{K_s} if attributed to extinction. Such uncertainties in $A_{K_s}(r)$ will have a modest impact on the derived RC distances.

Considering the prevailing inside-out scenario for disk formation and the significant evidence for gradients in both mean age and mean metallicity across spirals (e.g., MacArthur et al. 2004, González Delgado et al. 2015), problem *c* remains the most serious: It implies that the RC generally does not produce an unbiased measurement of the total stellar density, at least not in the thin disk where the youngest RC stars (1 to 4 Gyr) are present everywhere and in varying proportions. As far as we are aware, this effect has not been properly assessed in works dealing with the MW disk structure. In an old thick disk and Bulge, however, this specific problem does not exist.

4.4. RC Stars as Kinematical and Chemical-Evolution Probes

In large spectroscopic surveys, RC stars are the giants with the best possible distance estimates; hence, they are very useful kinematical and chemical-evolution probes. The advantage of using RC stars over dwarfs (such as the G dwarfs used by Jurić et al. 2008, Ivezić et al. 2012) is that they can probe much larger distances. Pavel (2014) even suggests the use of the RC as a probe of the magnetic field with distance.

RC stars are now being used extensively to interpret RAVE (Williams et al. 2013) and APOGEE data (Bovy et al. 2014, Nidever et al. 2014, López-Corredoira 2014, López-Corredoira et al. 2014). The main concerns with these analyses are essentially the same as for the density distributions: RC samples derived from spectroscopic data alone will contain a significant RGB (and RGB bump) contamination and will preferentially sample relatively young ages (1 to 4 Gyr) in the MW disk. This second aspect might be particularly frustrating, because in the absence of individual age estimates and space-resolved star-formation histories (SFHs), it does not allow a straightforward interpretation of the metallicity distributions derived from RC stars. A way out of this problem, however, is possible for the fields with asteroseismic information; they are the only cases in which stellar ages of field RC stars (and red giants in general) can be derived with good accuracy (Miglio et al. 2013).

In the Bulge, complications derived from the age spread of RC stars are much reduced, if not absent. In the wake of the first *Hipparcos* identification of nearby RC stars, Mao & Paczyński (2002) and Sumi et al. (2003) have proposed to measure streaming motions in the Bulge using RC stars. Such suggestions have so far produced modest conclusions (Rattenbury et al. 2007), mainly because of the large error bars still involved in OGLE-II proper motions.

4.5. RC Stars as Age Probes

Other authors have used RC stars as probes of the evolution of nearby galaxies. Particularly interesting was the suggestion by Hatzidimitriou (1991) to use the RC to provide a bulk mean age for the intermediate-age populations. The suggestion came from the observed linear relationship between the RGB-RC color separation and age in open clusters in the MW and in the Magellanic Clouds. The same relation is well predicted in evolutionary models by Girardi (1999)—at least for metallicities below the solar one.

The Hatzidimitriou (1991) method has been little used and was finally superseded by modern CMD-reconstruction methods that derive the best-fitting SFHs of nearby galaxies using the entire observed CMD. Classic examples of these methods are described by Harris & Zaritsky (2001) and Dolphin (2002). For galaxies at increasingly larger distances, the oldest part of the MSTOs can hardly be observed (even with HST for $d \gtrsim 100$ kpc), and hence the only old stellar populations present in the CMDs come from the RGB and RC, and from a handful of AGB stars. In these cases, the simulations by Dolphin (2002) demonstrate that the old SFH can still be recovered, thanks to the age sensitivity of the RC-to-RGB number ratio. This is a fortunate situation, but, contrastingly, it requires these CMD-reconstruction methods to be based on stellar models with reliable RGB and RC lifetimes. This is still not exactly the case for the RC (see Section 5.2), which can still be affected by errors of up to $\sim 20\%$. Therefore, significant systematic errors can still be affecting the SFH determination for these more distant galaxies.

5. OPEN ISSUES

From the discussion in the previous sections, it is clear that we have a fairly good understanding of RC behavior as a function of population age and metallicity, despite the possible significant systematic offsets in magnitude with respect to the data, and the difficulties in collecting data samples that can clearly constrain the model predictions. In these aspects, *Gaia* parallaxes and asteroseismic data will certainly greatly help to improve the situation in the coming years. In this section, we discuss possible ways to develop more efficient “red clump methods,” and the persistent difficulties in modeling convection during the final stages of CHeB. Neither of these topics is critical, in the sense that they do not represent any fundamental failure in the present uses of RC stars in the literature. However, they represent the likely forefronts to improve the use of RC stars in the years to come.

5.1. How Good a Standard Candle Can the RC Ever Become?

Since Paczyński & Stanek (1998), RC stars have been qualified as providing anything between “very precise” and “non-reliable” absolute distances. Certainly, a great part of the suspicion that accompanies RC distances comes from a single unknown: population corrections. Were they known a priori, errors in distances to Local Group galaxies would be reduced down to a few hundred magnitudes, reflecting the small uncertainties in the absolute calibration from *Hipparcos*, as well as the usual complications due to the interstellar extinction.

As recalled by Girardi & Salaris (2001), population corrections arise from the fact that RC stars are actually quite heterogeneous in nature: They span a very wide range of initial masses and metallicities, namely the entire interval from 1 to 10 Gyr, hence registering the almost complete chemical evolution of a galaxy and its wide temporal variations in SFRs—although being more sensitive to the 1–4-Gyr age range. Over these wide intervals of age (or initial mass), the RC includes stars with a common origin that have reached the tip of the RGB and developed the

He-flash at a well-defined He-core mass, and—in galaxies with young stellar populations—a significant fraction of SRC intruders. Even for the genuine RC stars that passed through the He-flash, their luminosities are not simply a function of the (almost-constant) He-core mass; they are also due to the H-burning shell, whose luminosity is sensitive to the envelope mass and not constant at all—the L_H/L_{He} average ratio varying in the range from ~ 0.35 to 4 among RC stars of different masses and metallicities.

By contrast, in favor of their standard-candle character, we have (*a*) their large numbers in the *Hipparcos* sample, which provides a very accurate reference absolute magnitude, and (*b*) their ubiquity and easy observability in nearby galaxies. These large numbers, however, result from the same factors that make them very heterogeneous, as just mentioned.

Therefore, RC stars are far from defining the ideal standard candles meant in classical textbooks. This warns us that distance determinations conducted with the RC—and especially the absolute ones—should be taken with due caution and generally not considered as superior to distances obtained with standard candles for which the absolute calibration is of an inferior statistical quality, like classical Cepheids or RR Lyrae.

On the practical side, the fundamental problem is that one needs to know the SFH of a galaxy to estimate the population correction ΔM_{λ} in Equation 8—but this is not possible without deep photometry and a detailed quantitative analysis of the entire CMD. In addition, the distance determinations should include the error caused by the SFH uncertainties, but this is almost never done (with few exceptions, e.g., Salaris & Girardi 2002). For this reason, the systematic errors in RC distances are very often underestimated.

Other, smaller problems are present in the RC distance methods: In crowded data, or in the MW field, the contamination by RGB stars is not negligible. The RGB background is often modeled by means of a second-order polynomial, but this is a crude approximation, given that the LF break caused by the RGB bump falls in the same magnitude interval as the RC. So one may wonder whether the method of fitting Equation 7 to the LF should not be replaced by the χ^2 fitting of model LFs, for both RC and RGB backgrounds—although, again, this requires assumptions about the underlying SFH.

Because knowledge of the SFH is so clearly needed to improve RC distance determinations, as well as the unavoidable use of stellar models, one may also take a step further in this exercise and ask whether RC distance determinations should not be plainly replaced by CMD-reconstruction methods that find the best fit of the entire CMD, including the RC and all the age-metallicity-dependent features at the RGB and MS, with stellar population models. Such methods are quite well developed, and available software packages (e.g., Harris & Zaritsky 2001, Dolphin 2002, Rubele et al. 2012) are already set to explore a range in distances and extinctions and to identify the values of these parameters that maximize the likelihood. Because the RC is usually the sharpest feature in the CMD, it turns out that the best-fitting distance will strongly depend on the RC position, and, moreover, it will have already taken the RC dependence on the SFH into consideration. This procedure goes against the idea of simple one-step methods for distance determinations, but it would clearly represent a better use of photometric data and of the maximum-likelihood concept—with the bonus of providing useful information about the SFH and extinction of the external galaxies, other than the distances. Indeed, this author is firmly convinced that this is the direction toward which many of the RC methods will evolve. Paradoxically, the RC might become an even better distance indicator the day it is denied any special status and is analyzed together with all the possible contaminants in the CMD.

Were this approach ever accepted as a replacement of the more simple RC distance methods, a main difficulty would be that a solution would also be required to verify the local calibration

by *Hipparcos*—which is still risky considering the large uncertainties in the SFH of the Solar Neighborhood but might become less of a problem in the *Gaia* era.

5.2. Pending Stellar-Evolution Issues: Mixing in Late He-Burning Stages, Mass Loss, Rotation, and Binarity

As discussed in numerous articles (e.g., Castellani et al. 2000, Bossini et al. 2015, Bressan et al. 2015, Constantino et al. 2015), there are still significant uncertainties in the evolution of CHeB stars; most of these uncertainties are related to the extension of convective regions. An increased MS core overshooting reduces M_{HeF} , hence changing the mass sequence of most stars observed at the RC and SRC, i.e., it will affect the relation between M_i and M_{core}^0 (and all quantities that depend on M_{core}^0) in the entire interval $1 M_{\odot} \lesssim M_i \lesssim M_{\text{HeF}} + 0.3 M_{\odot}$. Furthermore, core overshooting during the CHeB phase tends to increase its lifetime (Bressan et al. 1986).

Other significant changes in the CHeB lifetimes are caused by the uncertain mixing processes occurring at the end of this phase. Semiconvection (Castellani et al. 1971) and breathing pulses (Castellani et al. 1985) increase the He-fuel budget available during a final period in which the reaction $^{12}\text{C}(\alpha, \gamma)^{16}\text{O}$ is effective at the center—so, in addition, the uncertain $^{12}\text{C}(\alpha, \gamma)^{16}\text{O}$ rate becomes a critical input (Straniero et al. 2003). However, both semiconvection and breathing pulses become less effective if core overshooting is efficient, as demonstrated by Bressan et al. (1986). With present, well-accepted prescriptions of “moderate convective overshooting”—which means extending the core about 0.2 pressure scale heights above the classical Schwarzschild border, as adopted in popular sets of stellar models (Girardi et al. 2000a, Pietrinferni et al. 2004, Bressan et al. 2012)—low-mass CHeB lifetimes differ typically by less than 20% (see appendix in Girardi et al. 2013). Without entering into the details of these many calculations, we might simply assume this $\sim 20\%$ as being the present uncertainty in τ_{He} .

Perspectives of observationally constraining such mixing processes come from two fronts: (a) from the classical work of fitting the star counts and luminosities of RC stars in star clusters and (b) from asteroseismology of field RC stars. Surprisingly, the second front seems much closer to providing conclusive constraints to CHeB models. Constantino et al. (2015) and Bossini et al. (2015) describe quite exhaustively the effects of several mixing prescriptions in the asymptotic period spacing $\Delta\Pi_1$ and in the EAGB bump luminosity. The preliminary comparisons with *Kepler* data by Bossini et al. (2015) clearly favor models with a moderate overshooting region holding an adiabatic thermal stratification.

Another frequently mentioned uncertainty in RC evolution regards the mass loss at the previous RGB phase, which affects the relationship between the observed (turnoff) ages and the mass of RC stars. This uncertainty affects mainly the extreme metal-rich and lowest-mass RC stars, with $Z \gtrsim 0.5 Z_{\odot}$ and $M_i \lesssim 0.9 M_{\odot}$ (Girardi 1999), respectively; they are the only ones for which classical mass-loss formulas (Reimers 1975, Renzini & Fusi Pecci 1988) can produce an appreciable mass loss (a few $0.1 M_{\odot}$) close to their tip of the red giant branches. Even so, the predicted absolute magnitude of RC stars can be appreciably affected (Figure 6). However, some recent results (Heyl et al. 2015, Miglio et al. 2012) point to a reduced efficiency of RGB mass loss with respect to the classical values derived from old and metal-poor globular clusters. In any case, the situation is far from settled.

Then, additional uncertainties come from the effects of fast rotation and binarity in the life and appearance of RC stars. This is by far the most uncertain area, for which the observations of very populous intermediate-age Magellanic Cloud clusters, and the controversy about the origin of their eMSTOs and dual RCs, might be crucial (see Section 3.7). Large sets of suitable low-mass CHeB models, including both rotation and binaries, however, are still not available.

6. CLOSING REMARKS

This article provides a generic view of many subjects related to RC stars, essentially spanning from the very optimistic view of the RC being an excellent and single-step distance indicator, as advocated in the seminal work by Paczyński & Stanek (1998), to a more pessimistic view that considers the several contaminants, population effects, and age-metallicity sampling biases present in any sample of RC (or candidate RC) stars, which have to be faced in order to reduce the errors intrinsic to any RC method. Of course, between both views there is ample room for pragmatic approaches to derive improved results for the distributions of stellar parameters in our Galaxy and in nearby galaxies. The essential points to keep in mind, in our view, are the following:

1. RC stars span wide ranges of ages and metallicities. Though this is responsible for their large numbers and ubiquity in galaxies, it also makes them prone to population effects in their mean colors and magnitudes and, hence, not very accurate as distance and reddening indicators as is often claimed.
2. Their age distribution is heavily weighted toward ages smaller than a few gigayears, so their mean metallicities are not ideal to probe either the entire chemical evolution of galaxies or the kinematics of the oldest disk populations.
3. Model uncertainties in their lifetimes and luminosities might still be as high as 20% and 0.2 mag, respectively. These are quite significant errors considering their weight in detailed works of CMD fitting of star clusters and in the SFH recovery of nearby galaxies via the reconstruction of their CMDs.

Therefore, more steps are necessary in order to correct and improve the results of any RC method. We even advocate, provocatively (Section 5.1), that the best use of RC stars might pass through CMD fitting using maximum-likelihood methods that ultimately deny RC stars any special treatment as compared to other stars, and require the use of stellar models, in order to properly consider contaminants and population effects. This view applies more clearly to the use of the RC as a distance indicator to nearby galaxies, but it is obvious that other RC methods (e.g., their use as density indicators, as relative distance indicators, or as kinematic and chemical probes) could also benefit from maximum-likelihood approaches.

Whatever the research directions are to be taken in the upcoming years, we foresee a brilliant future for RC stars given the expectations we have on data from ongoing and planned surveys, as summarized below.

FUTURE ISSUES

1. *Gaia* parallaxes and stellar parameters (de Bruijne 2012, Michalik et al. 2015) will immensely increase the database of accurate absolute data for RC stars, allowing us to verify the behavior and fine details of the RC morphology expected from stellar models and definitively fix the zero-points of the RC absolute magnitude (both for the Solar Vicinity and in open clusters). However, they will not eliminate population effects in external galaxies and their dependence on their SFHs.
2. After 2020, LSST (Ivezić et al. 2008) will greatly improve the photometry and parallaxes for faint RC stars (Ivezić et al. 2015).
3. The greatest-ever revolution in the knowledge of RC stars, however, seems to be already underway, with the internal exploration of stars by massive asteroseismic surveys. The PLAnetary Transits and Oscillations of stars (Rauer et al. 2014), the Transiting Exoplanet

Survey Satellite (Ricker et al. 2014), and the second phase of *Kepler* (K2; Stello et al. 2015) are expected to sample and measure the intrinsic properties (masses, radii, distances, and especially ages) of RC stars much more extensively across the MW than *Kepler* and CoRoT. Although just a fraction of such data will allow $\Delta\Pi_1$ measurements, understanding of other asteroseismic parameters ($\Delta\nu$, v_{\max}) will hopefully be mature enough to fulfill the expectancies of doing Galactic archaeology with large samples of asteroseismic targets (Miglio et al. 2013).

4. Finally, near-IR imaging using large telescopes from space (e.g., WFIRST after 2024; Spergel et al. 2013) might reveal RC stars all over the Galaxy, largely avoiding the incompleteness and severe crowding that affects present ground-based surveys of the Bulge and Galactic midplane.

DISCLOSURE STATEMENT

The author is not aware of any affiliations, memberships, funding, or financial holdings that might be perceived as affecting the objectivity of this review.

ACKNOWLEDGMENTS

It is a pleasure to acknowledge the many friends and collaborators with whom I have shared RC data and thoughts, especially Eduardo Balbinot, Giampaolo Bertelli, Diego Bossini, Jo Bovy, Cesare Chiosi, Julianne Dalcanton, Patrick Eggenberger, Ortwin Gerhard, Paul Goudsroij, Martin Groenewegen, Leandro Kerber, Josefina Montalbán, Andrea Miglio, David Nidever, Thaise Rodrigues, Philip Rosenfield, Stefano Rubele, Maurizio Salaris, Basilio Santiago, Keivan Stassun, Ben Tatton, Jacco van Loon, Achim Weiss, Ben Williams, and Simone Zaggia. But my warmest thanks go to Alessandro Bressan and Paola Marigo, who allowed my RC work to evolve into its “third millennium state of the art” with the PARSEC code. Finally, thanks to the Laboratório Inter-institucional de e-Astronomia and Instituto de Física da Universidade Federal do Rio Grande do Sul staff for their warm hospitality during several visits in which this review was partially written with funding from the Brazilian agency Conselho Nacional de Desenvolvimento Científico e Tecnológico. Other partial funding came from the Università di Padova (Progetto di Ateneo 2012, ID: CPDA125588/12) and from PRIN INAF 2014 (CRA 1.05.01.94.05).

LITERATURE CITED

- Ahn CP, Alexandroff R, Allende Prieto C, et al. 2014. *Ap. J. Suppl.* 211:17
Alcock C, Allsman RA, Alves D, et al. 1997. *Ap. J.* 479:119–46
Alves DR. 2000. *Ap. J.* 539:732–41
Alves DR, Rejkuba M, Minniti D, Cook KH. 2002. *Ap. J. Lett.* 573:L51–54
Anderson E, Francis C. 2012. *Astron. Lett.* 38:331–46
Aparicio A, Gallart C. 2004. *Astron. J.* 128:1465–77
Bailey SI. 1902. *Ann. Harv. Coll. Obs.* 38:1
Balbinot E, Santiago BX, Girardi L, et al. 2015. *MNRAS* 449:1129–45
Bastian N, de Mink SE. 2009. *MNRAS* 398:L11–15
Bastian N, Niederhofer F. 2015. *MNRAS* 448:1863–73
Bastien FA, Stassun KG, Basri G, Pepper J. 2013. *Nature* 500:427–30
Beaulieu JP, Sackett PD. 1998. *Astron. J.* 116:209–19

- Beck PG, Bedding TR, Mosser B, et al. 2011. *Science* 332:205
- Bedding TR, Mosser B, Huber D, et al. 2011. *Nature* 471:608–11
- Bellazzini M, Ibata R, Martin N, et al. 2006. *MNRAS* 366:865–83
- Bica E, Geisler D, Dottori H, et al. 1998. *Astron. J.* 116:723–37
- Bildsten L, Paxton B, Moore K, Macias PJ. 2012. *Ap. J. Lett.* 744:L6
- Bland-Hawthorn J, Gerhard O. 2016. *Annu. Rev. Astron. Astrophys.* 54:529–96
- Bossini D, Miglio A, Salaris M, et al. 2015. *MNRAS* 453:2290–301
- Bovy J, Nidever DL, Rix HW, et al. 2014. *Ap. J.* 790:127
- Brandt TD, Huang CX. 2015. *Ap. J.* 807:25
- Bressan A, Bertelli G, Chiosi C. 1986. *Mem. Soc. Astron. Ital.* 57:411–26
- Bressan A, Girardi L, Marigo P, Rosenfield P, Tang J. 2015. *Astrophys. Space Sci. Proc.* 39:25
- Bressan A, Marigo P, Girardi L, et al. 2012. *MNRAS* 427:127–45
- Broomhall AM, Miglio A, Montalbán J, et al. 2014. *MNRAS* 440:1828–43
- Cabrera-Lavers A, González-Fernández C, Garzón F, Hammersley PL, López-Corredoira M. 2008. *Astron. Astrophys.* 491:781–87
- Cannon RD. 1970. *MNRAS* 150:111–35
- Cao L, Mao S, Nataf D, Rattenbury NJ, Gould A. 2013. *MNRAS* 434:595–605
- Castellani V, Chieffi A, Tornambe A, Pulone L. 1985. *Ap. J.* 296:204–12
- Castellani V, Degl'Innocenti S, Girardi L, Marconi M, Prada Moroni PG, Weiss A. 2000. *Astron. Astrophys.* 354:150–56
- Castellani V, Giannone P, Renzini A. 1971. *Ap. Space Sci.* 10:355–62
- Castelli F, Kurucz RL. 2003. In *Modelling of Stellar Atmospheres, Proc. IAU Symposium*, ed. N Piskunov, WW Weiss, DF Gray, 210:A20. Cambridge, UK: Cambridge Univ. Press
- Chaplin WJ, Miglio A. 2013. *Annu. Rev. Astron. Astrophys.* 51:353–92
- Cioni MRL, Clementini G, Girardi L, et al. 2011. *Astron. Astrophys.* 527:A116
- Cole AA. 1998. *Ap. J. Lett.* 500:L137–40
- Constantino T, Campbell SW, Christensen-Dalsgaard J, Lattanzio JC, Stello D. 2015. *MNRAS* 452:123–45
- Corsi CE, Buonanno R, Fusi Pecci F, et al. 1994. *MNRAS* 271:385–420
- Crowl HH, Sarajedini A, Piatti AE, et al. 2001. *Astron. J.* 122:220–31
- Dalcanton JJ, Williams BF, Lang D, et al. 2012. *Ap. J. Suppl.* 200:18
- Dalcanton JJ, Williams BF, Seth AC, et al. 2009. *Ap. J. Suppl.* 183:67–108
- de Bruijne JHJ. 2012. *Ap. Space Sci.* 341:31–41
- De Marchi G, Panagia N, Girardi L. 2014. *MNRAS* 438:513–28
- Dolphin AE. 2002. *MNRAS* 332:91–108
- D’Orazi V, Bragaglia A, Tosi M, Di Fabrizio L, Held EV. 2006. *MNRAS* 368:471–78
- Eggenberger P, Miglio A, Montalban J, et al. 2010. *Astron. Astrophys.* 509:A72
- Ferraro FR, Dalessandro E, Mucciarelli A, et al. 2009. *Nature* 462:483–86
- Ferraro FR, Origlia L, Testa V, Maraston C. 2004. *Ap. J.* 608:772–80
- Francis C, Anderson E. 2014. *MNRAS* 441:1105–14
- Gallart C, Freedman WL, Mateo M, et al. 1999. *Ap. J.* 514:665–74
- Gallart C, Zoccali M, Aparicio A. 2005. *Annu. Rev. Astron. Astrophys.* 43:387–434
- Gardiner LT, Hatzidimitriou D. 1992. *MNRAS* 257:195–224
- Gardiner LT, Hawkins MRS. 1991. *MNRAS* 251:174–91
- Girardi L. 1999. *MNRAS* 308:818–32
- Girardi L, Bressan A, Bertelli G, Chiosi C. 2000a. *Astron. Astrophys. Suppl.* 141:371–83
- Girardi L, Eggenberger P, Miglio A. 2011. *MNRAS* 412:L103–7
- Girardi L, Groenewegen MAT, Hatziminaoglou E, da Costa L. 2005. *Astron. Astrophys.* 436:895–915
- Girardi L, Groenewegen MAT, Weiss A, Salaris M. 1998. *MNRAS* 301:149–60
- Girardi L, Marigo P, Bressan A, Rosenfield P. 2013. *Ap. J.* 777:142
- Girardi L, Mermilliod JC, Carraro G. 2000b. *Astron. Astrophys.* 354:892–98
- Girardi L, Rubele S, Kerber L. 2009. *MNRAS* 394:L74–78
- Girardi L, Salaris M. 2001. *MNRAS* 323:109–29
- Gonzalez OA, Rejkuba M, Minniti D, et al. 2011. *Astron. Astrophys.* 534:L14

- González Delgado RM, García-Benito R, Pérez E, et al. 2015. *Astron. Astrophys.* 581:A103
- Goudfrooij P, Girardi L, Kozhurina-Platais V, et al. 2014. *Ap. J.* 797:35
- Goudfrooij P, Girardi L, Rosenfield P, et al. 2015. *MNRAS* 450:1693–704
- Goudfrooij P, Puzia TH, Chandar R, Kozhurina-Platais V. 2011. *Ap. J.* 737:4
- Grocholski AJ, Sarajedini A. 2002. *Astron. J.* 123:1603–12
- Grocholski AJ, Sarajedini A, Olsen KAG, Tiede GP, Mancone CL. 2007. *Astron. J.* 134:680–93
- Groenewegen MAT. 2008. *Astron. Astrophys.* 488:935–41
- Harris J, Zaritsky D. 2001. *Ap. J. Suppl.* 136:25–40
- Haschke R, Grebel EK, Duffau S. 2011. *Astron. J.* 141:158
- Hatzidimitriou D. 1991. *MNRAS* 251:545–54
- Hekker S, Gilliland RL, Elsworth Y, et al. 2011. *MNRAS* 414:2594–601
- Heyl J, Kalirai J, Richer HB, et al. 2015. *Ap. J.* 810:127
- Holtzman JA, Mould JR, Gallagher JS III, et al. 1997. *Astron. J.* 113:656–68
- Holtzman JA, Smith GH, Grillmair C. 2000. *Astron. J.* 120:3060–69
- Huber D, Bedding TR, Stello D, et al. 2010. *Ap. J.* 723:1607–17
- Ibata RA, Lewis GF, Beaulieu JP. 1998. *Ap. J. Lett.* 509:L29–32
- Ivezić Ž, Beers TC, Jurić M. 2012. *Annu. Rev. Astron. Astrophys.* 50:251–304
- Ivezić Ž, Kahn SM, Eliason P. 2015. *EAS Publ. Ser.* 67–68:211–17
- Ivezić Z, Tyson JA, Abel B, et al. 2008. *LSST: From Science Drivers to Reference Design and Anticipated Data Products.* Work. Pap., Dep. Astron., Univ. Wash. arXiv:0805.2366
- Jurić M, Ivezić Ž, Brooks A, et al. 2008. *Ap. J.* 673:864–914
- Kallinger T, Mosser B, Hekker S, et al. 2010. *Astron. Astrophys.* 522:A1
- Kato D, Nagashima C, Nagayama T, et al. 2007. *Publ. Astron. Soc. Jpn.* 59:615–41
- Kroupa P. 2002. *Science* 295:82–91
- Laney CD, Joner MD, Pietrzyński G. 2012. *MNRAS* 419:1637–41
- López-Corredoira M. 2006. *MNRAS* 369:1911–15
- López-Corredoira M. 2014. *Astron. Astrophys.* 563:A128
- López-Corredoira M, Abedi H, Garzón F, Figueras F. 2014. *Astron. Astrophys.* 572:A101
- López-Corredoira M, Cabrera-Lavers A, Garzón F, Hammersley PL. 2002. *Astron. Astrophys.* 394:883–99
- López-Corredoira M, Momany Y, Zaggia S, Cabrera-Lavers A. 2007. *Astron. Astrophys.* 472:L47–50
- MacArthur LA, Courteau S, Bell E, Holtzman JA. 2004. *Ap. J. Suppl.* 152:175–99
- Mao S, Paczyński B. 2002. *MNRAS* 337:895–900
- Massari D, Mucciarelli A, Ferraro FR, et al. 2014. *Ap. J.* 795:22
- McQuinn KBW, Skillman ED, Dolphin A, et al. 2015. *Ap. J.* 812:158
- McWilliam A, Zoccali M. 2010. *Ap. J.* 724:1491–502
- Mermilliod JC, Mathieu RD, Latham DW, Mayor M. 1998. *Astron. Astrophys.* 339:423–30
- Mermilliod JC, Mayor M. 1990. *Astron. Astrophys.* 237:61–72
- Mermilliod JC, Mayor M, Udry S. 2008. *Astron. Astrophys.* 485:303–14
- Michalik D, Lindegren L, Hobbs D. 2015. *Astron. Astrophys.* 574:A115
- Miglio A, Brogaard K, Stello D, et al. 2012. *MNRAS* 419:2077–88
- Miglio A, Chiappini C, Morel T, et al. 2013. *MNRAS* 429:423–28
- Miglio A, Montalbán J, Baudin F, et al. 2009. *Astron. Astrophys.* 503:L21–24
- Minniti D, Saito RK, Alonso-García J, Lucas PW, Hempel M. 2011. *Ap. J. Lett.* 733:L43
- Minniti D, Saito RK, Gonzalez OA, et al. 2014. *Astron. Astrophys.* 571:A91
- Mocák M, Müller E, Weiss A, Kifonidis K. 2009. *Astron. Astrophys.* 501:659–77
- Monachesi A, Trager SC, Lauer TR, et al. 2011. *Ap. J.* 727:55
- Montalbán J, Miglio A, Noels A, et al. 2013. *Ap. J.* 766:118
- Mosser B, Barban C, Montalbán J, et al. 2011. *Astron. Astrophys.* 532:A86
- Mosser B, Belkacem K, Goupil MJ, et al. 2010. *Astron. Astrophys.* 517:A22
- Mosser B, Benomar O, Belkacem K, et al. 2014. *Astron. Astrophys.* 572:L5
- Mosser B, Goupil MJ, Belkacem K, et al. 2012. *Astron. Astrophys.* 548:A10
- Munari U, Henden A, Frigo A, et al. 2014. *Astron. J.* 148:81
- Nataf DM, Gould A, Fouqué P, et al. 2013. *Ap. J.* 769:88

- Nataf DM, Udalski A, Gould A, Fouqué P, Stanek KZ. 2010. *Ap. J. Lett.* 721:L28–32
- Nataf DM, Udalski A, Skowron J, et al. 2015. *MNRAS* 447:1535–49
- Ness M, Freeman K, Athanassoula E, et al. 2013. *MNRAS* 430:836–57
- Nidever DL, Bovy J, Bird JC, et al. 2014. *Ap. J.* 796:38
- Nidever DL, Monachesi A, Bell EF, et al. 2013. *Ap. J.* 779:145
- Nishiyama S, Nagata T, Sato S, et al. 2006. *Ap. J.* 647:1093–98
- Nishiyama S, Tamura M, Hatano H, et al. 2009. *Ap. J.* 696:1407–17
- Olszewski EW, Suntzeff NB, Mateo M. 1996. *Annu. Rev. Astron. Astrophys.* 34:511–50
- Paczyński B, Stanek KZ. 1998. *Ap. J. Lett.* 494:L219–22
- Pavel MD. 2014. *Astron. J.* 148:49
- Percival SM, Salaris M. 2003. *MNRAS* 343:539–46
- Perryman MAC, Lindegren L, Kovalevsky J, et al. 1997. *Astron. Astrophys.* 323:L49–52
- Piatti AE, Geisler D, Bica E, et al. 1999. *Astron. J.* 118:2865–74
- Pietrinferni A, Cassisi S, Salaris M, Castelli F. 2004. *Ap. J.* 612:168–90
- Pietrzyński G, Górska M, Gieren W, et al. 2010. *Astron. J.* 140:1038–42
- Pinsonneault MH, Elsworth Y, Epstein C, et al. 2014. *Ap. J. Suppl.* 215:19
- Popowski P, Griest K, Thomas CL, et al. 2005. *Ap. J.* 631:879–905
- Rattenbury NJ, Mao S, Debattista VP, et al. 2007. *MNRAS* 378:1165–76
- Rauer H, Catala C, Aerts C, et al. 2014. *Exp. Astron.* 38:249–330
- Reimers D. 1975. *Mem. Soc. R. Sci. Liege* 8:369–82
- Renzini A, Buzzoni A. 1986. In *Spectral Evolution of Galaxies*, ed. C Chiosi, A Renzini. *Astrophys. Space Sci. Libr.* 122:195–235. Dordrecht, Neth.: Reidel
- Renzini A, Fusi Pecci F., 1988. *Annu. Rev. Astron. Astrophys.* 26:199–244
- Ricker GR, Winn JN, Vanderspek R, et al. 2014. In *Space Telescopes and Instrumentation 2014: Optical, Infrared, and Millimeter Wave*, ed. JM Oschmann, M Clampin, GG Fazio, HA MacEwen. *Proc. SPIE Conf. Ser.* 9143:914320. Bellingham, WA: SPIE
- Ripepi V, Cignoni M, Tosi M, et al. 2014. *MNRAS* 442:1897–921
- Robin AC, Reylé C, Derrière S, Picaud S. 2003. *Astron. Astrophys.* 409:523–40
- Rodrigues TS, Girardi L, Miglio A, et al. 2014. *MNRAS* 445:2758–76
- Rubele S, Kerber L, Girardi L, et al. 2012. *Astron. Astrophys.* 537:A106
- Saito RK, Minniti D, Dias B, et al. 2012. *Astron. Astrophys.* 544:A147
- Saito RK, Zoccali M, McWilliam A, et al. 2011. *Astron. J.* 142:76
- Salaris M, Girardi L. 2002. *MNRAS* 337:332–40
- Salpeter EE. 1955. *Ap. J.* 121:161
- Sandquist EL. 2004. *MNRAS* 347:101–18
- Sarajedini A, Dotter A, Kirkpatrick A. 2009. *Ap. J.* 698:1872–78
- Sarajedini A, von Hippel T, Kozhurina-Platais V, Demarque P. 1999. *Astron. J.* 118:2894–907
- Silva Aguirre V, Ruchti GR, Hekker S, et al. 2014. *Ap. J. Lett.* 784:L16
- Skowron DM, Jacyszyn AM, Udalski A, et al. 2014. *Ap. J.* 795:108
- Skrutskie MF, Cutri RM, Stiening R, et al. 2006. *Astron. J.* 131:1163–83
- Smecker-Hane TA, Stetson PB, Hesser JE, Lehnert MD. 1994. *Astron. J.* 108:507–13
- Spergel D, Gehrels N, Breckinridge J, et al. 2013. *Wide-Field InfraRed Survey Telescope-Astrophysics Focused Telescope Assets WFIRST-AFTA Final Report by the Science Definition Team (SDT) and WFIRST Study Office.* arXiv:1305.5422
- Stanek KZ. 1996. *Ap. J. Lett.* 460:L37
- Stanek KZ, Garnavich PM. 1998. *Ap. J. Lett.* 503:L131–34
- Stanek KZ, Mateo M, Udalski A, et al. 1994. *Ap. J. Lett.* 429:L73–76
- Stanek KZ, Udalski A, Szymański M, et al. 1997. *Ap. J.* 477:163–75
- Stanek KZ, Zaritsky D, Harris J. 1998. *Ap. J. Lett.* 500:L141–44
- Stello D, Huber D, Bedding TR, et al. 2013. *Ap. J. Lett.* 765:L41
- Stello D, Huber D, Sharma S, et al. 2015. *Ap. J. Lett.* 809:L3
- Straniero O, Domínguez I, Imbriani G, Piersanti L. 2003. *Ap. J.* 583:878–84
- Subramaniam A. 2005. *Astron. Astrophys.* 430:421–26

- Subramaniam A, Subramanian S. 2009. *Ap. J. Lett.* 703:L37–40
- Subramanian S, Subramaniam A. 2012. *Ap. J.* 744:128
- Sumi T, Eyer L, Woźniak PR. 2003. *MNRAS* 340:1346–52
- Sweigart AV, Greggio L, Renzini A. 1990. *Ap. J.* 364:527–39
- Tatton BL, van Loon JT, Cioni MR, et al. 2013. *Astron. Astrophys.* 554:A33
- Thomas HC. 1967. *Z. Astrophys.* 67:420
- Tinsley BM. 1980. *Fundam. Cosmic Phys.* 5:287–388
- Udalski A. 1998. *Acta Astron.* 48:383–404
- Valentini M, Munari U. 2010. *Astron. Astrophys.* 522:A79
- van Helschocht V, Groenewegen MAT. 2007. *Astron. Astrophys.* 463:559–65
- van Leeuwen F, ed. 2007. *Hipparcos, the New Reduction of the Raw Data*, Vol. 350, *Astrophysics and Space Science Library*. Dordrecht, Neth.: Springer
- van Leeuwen F. 2009. *Astron. Astrophys.* 497:209–42
- Wegg C, Gerhard O. 2013. *MNRAS* 435:1874–87
- Wegg C, Gerhard O, Portail M. 2015. *MNRAS* 450:4050–69
- Weisz DR, Dolphin AE, Skillman ED, et al. 2013. *MNRAS* 431:364–71
- Williams BF, Dalcanton JJ, Dolphin AE, Holtzman J, Sarajedini A. 2009. *Ap. J. Lett.* 695:L15–19
- Williams BF, Lang D, Dalcanton JJ, et al. 2014. *Ap. J. Suppl.* 215:9
- Williams MEK, Steinmetz M, Binney J, et al. 2013. *MNRAS* 436:101–21
- Wozniak PR, Stanek KZ. 1996. *Ap. J.* 464:233
- Yaz Gökçe E, Bilir S, ÖzTÜRKmen ND, et al. 2013. *New Astron.* 25:19–26
- Zaritsky D, Lin DNC. 1997. *Astron. J.* 114:2545
- Zasowski G, Johnson JA, Frinchaboy PM, et al. 2013. *Astron. J.* 146:81
- Zhao G, Qiu HM, Mao S. 2001. *Ap. J. Lett.* 551:L85–88
- Zwitter T, Matijević G, Breddels MA, et al. 2010. *Astron. Astrophys.* 522:A54

Contents

A Fortunate Half-Century <i>Jeremiah P. Ostriker</i>	1
The Remnant of Supernova 1987A <i>Richard McCray and Claes Fransson</i>	19
Astrophysics with Extraterrestrial Materials <i>Larry R. Nittler and Fred Ciesla</i>	53
Red Clump Stars <i>Léo Girardi</i>	95
Accretion onto Pre-Main-Sequence Stars <i>Lee Hartmann, Gregory Herczeg, and Nuria Calvet</i>	135
Interstellar Hydrides <i>Maryvonne Gerin, David A. Neufeld, and Javier R. Goicoechea</i>	181
The Quest for B Modes from Inflationary Gravitational Waves <i>Marc Kamionkowski and Ely D. Kovetz</i>	227
Gravitational Instabilities in Circumstellar Disks <i>Kaitlin Kratter and Giuseppe Lodato</i>	271
The Evolution of the Intergalactic Medium <i>Matthew McQuinn</i>	313
The Magellanic Stream: Circumnavigating the Galaxy <i>Elena D'Onghia and Andrew J. Fox</i>	363
Masses, Radii, and the Equation of State of Neutron Stars <i>Feryal Özel and Paulo Freire</i>	401
The Eccentric Kozai-Lidov Effect and Its Applications <i>Smadar Naoz</i>	441
Protostellar Outflows <i>John Bally</i>	491

The Galaxy in Context: Structural, Kinematic, and Integrated Properties <i>Joss Bland-Hawthorn and Ortwin Gerhard</i>	529
Structure and Kinematics of Early-Type Galaxies from Integral Field Spectroscopy <i>Michele Cappellari</i>	597
Six Decades of Spiral Density Wave Theory <i>Frank H. Shu</i>	667
Gamma-Ray Observations of Active Galactic Nuclei <i>Grzegorz (Greg) Madejski and Marek Sikora</i>	725
Galaxies in the First Billion Years After the Big Bang <i>Daniel P. Stark</i>	761

Indexes

Cumulative Index of Contributing Authors, Volumes 43–54	805
Cumulative Index of Article Titles, Volumes 43–54	808

Errata

An online log of corrections to *Annual Review of Astronomy and Astrophysics* articles may be found at <http://www.annualreviews.org/errata/astro>